SAR/ISAR data exploitation toolbox for focusing moving targets

T. Thayaparan
DRDC – Ottawa Research Centre

Defence Research and Development Canada
Scientific Report
DRDC-RDDC-2015-R018
March 2015

Abstract

The commonly used technique for SAR/ISAR imaging of a moving target is a Fourier-based image formation, which assumes time invariance of the Doppler frequency to resolve the image in the cross-range. However, in real-world ISAR/SAR imaging scenarios, when a target exhibits complex motion such as rotation, acceleration, or manoeuvring, standard Fourier-based methods can cause range-Doppler image blurring and leave the image unrecognizable. For target recognition applications, mainly those in military surveillance and reconnaissance operations, a blurred ISAR image of the moving target has to be refocused quickly so that it can be used for real-time target identification. Subsequently, advanced image focusing (or refocusing distorted images) methods such as, S-method, adaptive S-method and local polynomial Fourier transform method were developed. These three image focusing and motion compensation algorithms were successfully tested and validated with numerous measured ocean and air targets using airborne, space-borne, and ground-based sensors. Based on these three algorithms, the SAR/ISAR data exploitation toolbox was developed for Geospatial Intelligence (GEOINT) support to the Canadian Armed Forces (CAF).

Significance for defence and security

In SAR/ISAR (Synthetic Aperture Radar/Inverse ISAR) RADARSAT or airborne radar imaging scenarios, when a moving target exhibits complex motion such as rotation, acceleration, or manoeuvring, standard Fourier-based methods can cause range-Doppler image blurring and leave the image unrecognizable. In these scenarios, this toolbox can be applied to refocus the distorted image. The toolbox provides improved target detection and imaging. The toolbox will be incorporated into Image Analyst pro (IA pro), which will eventually be available to the CFJIC (Canadian Forces Joint Imagery Centre) and MCE (Mapping and Charting Establishment) clients. IA pro is DRDCŠs test bed system for validation and demonstration of new algorithms for SAR-based Geospatial Intelligence (GEOINT). The goal is the transition of a developed toolbox to operational status for the CAF.

Résumé

La technique couramment utilisée pour l'imagerie SAR ou ISAR d'une cible mobile est la formation d'images fondée sur la transformée de Fourier, ce qui suppose que le décalage Doppler utilisé pour augmenter la résolution de l'image dans l'axe transversal ne varie pas dans le temps. Toutefois, dans des scénarios réels d'imagerie SAR ou ISAR, lorsqu'une cible présente des mouvements complexes, comme une rotation, une accélération ou une manIJuvre, les méthodes standard fondées sur la transformée de Fourier peuvent produire un flou distance Doppler et rendre l'image méconnaissable. Pour les applications relatives à la reconnaissance de cibles, surtout les opérations militaires de surveillance et de reconnaissance, l'image ISAR floue d'une cible mobile doit être refocalisée rapidement pour servir à l'identification de cibles en temps réel. Des méthodes évoluées de focalisation d'images (ou de refocalisation d'images déformées), comme la méthode S, la méthode adaptative S et la méthode par transformée de Fourier polynomiale locale ont donc été mises au point. Ces trois algorithmes de focalisation d'images et de compensation du mouvement ont été testés et validés avec succès sur diverses cibles aériennes et océaniques mesurées au moyen de capteurs aériens, spatiaux et terrestres. À partir de ces trois algorithmes, la trousse dŠexploitation des données SAR ou ISAR a été conçue pour soutenir le renseignement géospatial (GEOINT) des Forces armées canadiennes (FAC).

Importance pour la défense et la sécurité

Dans les scénarios d'imagerie au moyen de SAR ou d'ISAR de RADARSAT ou au moyen de radars aéroportés, si une cible mobile présente des mouvements complexes, comme une rotation, une accélération ou une manIJuvre, les méthodes standard fondées sur la transformée de Fourier peuvent produire un flou distance Doppler et rendre l'image méconnaissable. Dans ces scénarios, la trousse peut être utilisée pour refocaliser l'image déformée. Cette trousse permet d'améliorer la détection et l'image de la cible. Elle est incluse dans l'outil Image Analyst pro (IA pro), qui sera éventuellement offert aux clients du Centre d'imagerie interarmées des Forces canadiennes (CIIFC) et du Service de cartographie (S Carto). IA pro est un système de banc d'essai de RDDC, et il est utilisé pour valider et démontrer de nouveaux algorithmes pour le renseignement géospatial (GEOINT) axé sur le SAR. L'objectif consiste à passer de la trousse développée à l'état opérationnel pour les FAC.

Table of contents

List of figures

This page intentionally left blank.

1 Introduction

Inverse synthetic aperture radar (ISAR) has a capability of obtaining fine resolution images of moving targets under all weather and all day from long ranges. It is an important method of target identification. ISAR and synthetic aperture radar (SAR), both utilize the range-Doppler principle to get the desired image. SAR, which is usually carried on aircraft, satellites and other moving platforms, is used to image terrain and maritime surveillance. ISAR can be operated from ground-based, spaceborne-based as well as airborne-based, and is used to image the aircraft, ships and ground moving targets. Different to SAR, the objects of ISAR are usually non-cooperative, i.e., the imaging parameters are unknown prior to image formation. The non-cooperation of the target introduces the main problem of not knowing the dynamics of the radar-target system during the coherent integration time. Such a limitation leads to the use of blind radial motion compensation and image formation processing that must deal with highly non-stationary signals [1–15]. In airborne ISAR imaging of ships, the sea-state changes frequently, and the radar is moving as well. The imaging difficulty is increased largely. Thus, the special study is needed for obtaining high-resolution images of ships, aircraft and ground targets.

One proven approach for achieving SAR/ISAR motion compensation and focused distorted SAR/ISAR images is based on high-resolution time-frequency-based approach. Several time–frequency (TF) techniques developed and successfully refocused blurred SAR/ISAR images [17-45]. This occurs because the images are obtained at a particular instant in time when the target's motion can be considered uniform. However, the data are not collected instantaneously. Consequently, a large number of refocused ISAR images will be generated, spanning the entire coherent integration time (CIT). For accurate target recognition, it is imperative to make use of only the best refocused image. It would be very impractical and inefficient for the image analyst to examine all of the images produced in order to identify which is the best. Such manual inspection, or even with the aid of an automated image searching algorithm, only adds extra complexity to the target recognition process. To overcome these computational complexities and computational burden, three innovative algorithms and methodologies were developed that can be used for operational by Canadian Armed Forces (CAF).

For target recognition applications, mainly those in military surveillance and reconnaissance operations, a blurred ISAR image has to be refocused quickly so that it can be used for real-time target identification. Three algorithms were developed that can be used for real-time operations; 1) S-method [22, 39], 2) adaptive S-method [42, 46], and 3) local polynomial Fourier transform [24, 41, 43, 47]. The S-method is a numerically simple, computationally fast, real-time method that significantly improves the focusing of distorted SAR/ISAR imagery of moving targets. The S-method achieves

motion compensation, image formation and image enhancement of ship targets in SAR and air targets in ISAR. This approach performs better than the Fourier transform (FT) by drastically improving images of fast, manoeuvring ship targets/air targets by increasing the signal-to-noise (SNR) in both low and high noise environments. These advantages are a result of the S-method's ability to automatically compensate for quadratic and all even higher-order terms in phase. Thus, targets with constant acceleration will undergo full motion compensation and their point scatterers will each be localized. It should be noted that the source of the quadratic term can come not only from acceleration, but also from non-uniform rotational motion and the cosine term in wide-angle imaging.

An efficient adaptive S-method-based approach was developed for imaging of SAR and ISAR targets. It is a post-processing technique, since the first stage is the standard radar imaging with the two-dimensional Fourier transform. It has been shown that simple strategy for adaptive selection of the frequency window width in the S-method produces excellent results with highly focused radar images and with avoiding undesired interference terms. The adaptive selection of frequency window width is an important part of the proposed technique. The automatic threshold determination was developed, and the procedure based on the Otsu algorithm appears to be very efficient.

The local polynomial Fourier transform-based (LPFT) algorithm for focusing SAR/ISAR images was developed. It produces a well-focused image of moving targets, without defocusing stationary targets or inducing undesired cross-terms. The algorithm can be performed in two modes: with second-order LPFT or with the order-adaptive LPFT. The algorithm performs accurately even in relatively high noise environments. It is based on the linear signal representation, and it can produce very high-resolution of the radar image with moving target that is close to the resolution of the FT for radar images with non-moving targets. The algorithm with order-adaptive form of the LPFT can compensate higher-order polynomials in the signal phase.

The S-method, adaptive S-method, and LPFT algorithms were tested and validated by numerous ground-based, spaceborne-based and airbourne-based imagery data sets, for example, RADARSAT-2, RADARSAT-1, TerraSAR-X, etc. [16–19, 48–50]. These algorithms were now integrated into a Matlab-based SAR/ISAR data exploitation toolbox. The analytical continuous wave (CW) radar signal model is given in Section 2. In Section 3, ISAR basic definitions and model are provided. ISAR image using the Fourier transform method is given in Section 4. The S-method-based improvement of radar image in provided in Section 5. In Section 6, adaptive S-method-based radar image is given while the local polynomial Fourier transform-based radar image is provided in Section 7. The illustration of a SAR/ISAR data exploitation toolbox is given in Section 8. In Section 8, the time-frequency toolbox is also illustrated.

2 Analytic CW radar signal model

For the analytic derivation of the model, consider a continuous wave (CW) radar that transmits a signal in the form of a coherent series of chirps [8]:

$$v_p(t) = \begin{cases} \exp(j\pi B f_r t^2) & \text{for} \quad 0 \leq t \leq T_r \\ 0 & \text{otherwise} \end{cases} \tag{1}$$

where T_r is the repetition time, $f_r = 1/T_r$ is the repetition frequency, and B is the emitted waveform bandwidth.

In one revisit, the transmitted signal consists of M such chirps:

$$v(t) = \exp(-j\omega_0 t) \sum_{m=0}^{M-1} v_p(t - mT_r) \tag{2}$$

where ω_0 is the radar operating frequency. The total signal duration is $T_c = MT_r$ and represents the CIT.

Consider a signal of form (2) transmitted toward a target. If the target distance from the radar is d (referred to as range), then the received signal is delayed with respect to the transmitted signal for $t_d = 2d/c$, where c is the velocity of propagation, equal to the speed of light. The phase of the received signal is changed as $\phi = 2kd = 4\pi d/\lambda = 4\pi d f_0/c = 2\omega_0 d/c$.

Thus, the form of the received signal is:

$$u(t) = \sigma \exp(j[-\omega_0(t - \frac{2d}{c})]) \sum_{m=0}^{M-1} v_p(t - \frac{2d}{c} - mT_r)$$

where σ is the reflection coefficient. The received signal is mixed (multiplied) with the complex-conjugate of the transmitted signal and shifted in time with a minimal delay T_0. We will assume that a constant distance is properly compensated and that $T_0 = 0$. Without loss of generality, we can consider only one component of the received signal:

$$q(m,t) = \sigma \exp(j\omega_0 \frac{2d}{c}) \exp(-j2\pi B f_r (t - mT_r) \frac{2d}{c}).$$

A two-dimensional discrete signal is obtained by sampling in time with $t - mT_r = nT_s$

$$q(m,n) = \sigma \exp(j\omega_0 \frac{2d}{c}) \exp(-j2\pi B f_r n T_s \frac{2d}{c}).$$

3 ISAR basic definitions and model

Inverse synthetic aperture radar (ISAR) is a method for obtaining high-resolution of a target based on the change in viewing angle of the target with respect to a fixed radar. An illustration of a target and relevant quantities is shown in Figure 1. Suppose that a target consists of P point scatterers whose locations are (x_p, y_p), $p = 1, 2, ..., P$, in the coordinate system whose center is the center of target rotation. The coordinate in the direction of the radar-target line (range coordinate) is denoted by x_p, while y_p is the coordinate in the normal direction to this line (cross-range coordinate). The target's total movement can be considered as a superposition of both translation and rotation.

Assume that the target moves along a straight line parallel to the ground at a height h, and that its ground distance from radar is z,meaning the range $d = \sqrt{h^2 + z^2}$. From the radar position the target is seen at an angle α, meaning $\sin(\alpha) = h/d$. In the next instant, $t + \Delta t$, the target is moved to the new position corresponding to the ground distance $z + \Delta z$, meaning the range $d = \sqrt{h^2 + (z + \Delta z)^2}$, and it is seen from the radar at an angle $\alpha + \Delta\alpha$. Thus, this movement can be considered as a translation for Δd and rotation for $\Delta\alpha$.

If the target speed is v_t then $\Delta z = v_t \Delta t$. Since

$$\alpha = \tan^{-1}(\frac{h}{z}) \text{ and } \frac{\partial\alpha}{\partial z} = \frac{-h}{z^2 + h^2}$$

we get:

$$\Delta\alpha \cong \frac{-h}{z^2 + h^2}\Delta z$$

or

$$\Delta\alpha \cong -(\Delta z)h/d^2 = -v_t(\Delta t)h/d^2.$$

During the considered time interval t the point scatterer rotates for $\theta_R(t) = \omega_R t$. The new coordinates of the scatterer are:

$$\begin{bmatrix} x'_p \\ y'_p \end{bmatrix} = \begin{bmatrix} \cos(\theta_R(t) & \sin(\theta_R(t)) \\ -\sin(\theta_R(t) & \cos(\theta_R(t)) \end{bmatrix} \begin{bmatrix} x_p \\ y_p \end{bmatrix}. \tag{3}$$

The total range position, for small $\theta_R(t) \to 0$, is:

$$\begin{aligned} d(t) &= \sqrt{(R + x'_p)^2 + y'^2_p} \cong R + x'_p \\ &= R + x_p \cos(\theta_R(t)) + y_p \sin(\theta_R(t)) \\ &\cong R + x_p. \end{aligned} \tag{4}$$

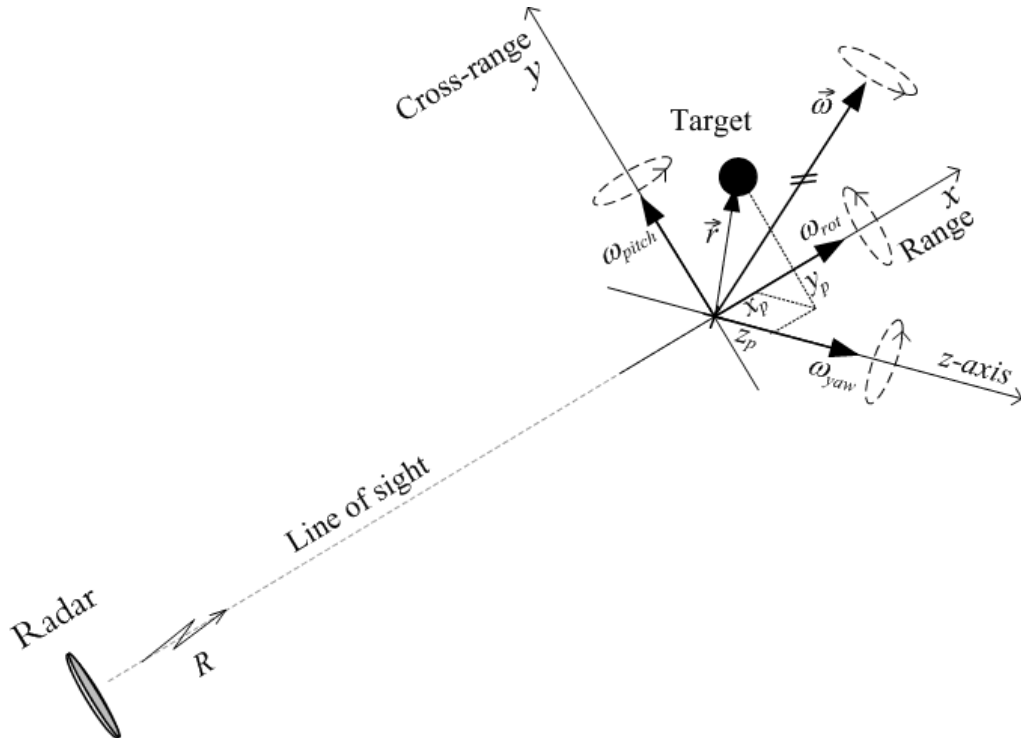

Figure 1: *Illustration of the ISAR principle.*

The range contains information about coordinate x_p, since for $\theta_R(t) = \omega_R t \to 0$ we get, $\cos(\theta_R(t)) \to 1$, $\sin(\theta_R(t)) \to \theta_R(t)$ and $d(t) \cong R + x_p + y_p\omega_R t$.

The Doppler shift is proportional to the velocity in the direction of the line-of-sight:

$$\Delta\omega_d \cong \frac{2\omega_0}{c}\frac{d}{dt}[d(t)] = \frac{2\omega_0}{c}\frac{d}{dt}[R + x_p\cos(\theta_R(t)) + y_p\sin(\theta_R(t))].$$

For $\theta_R(t) = \omega_R t \to 0$ again $d(t) \cong R + x_p + y_p\omega_R t$. Note that here we must not neglect the term $y_p\omega_R t$ since it is multiplied by a large number $2\omega_0/c$ in defining the phase of $\exp(j2\omega_0 d/c)$. Thus:

$$\Delta\omega_d = \frac{2\omega_0}{c}y_p\omega_R \sim y_p$$

assuming, in addition to the above approximations, that the translation is compensated, i.e., $R(t) = R$.

3.1 Nonuniform motion

In general, the target motion over M chirps in one revisit cannot be considered as linear with velocity $v = y_p\omega_R$. Even in the simplest case when the target rotates with a constant angular velocity ω_R, for a longer period of time, the line-of-sight (LOS) projection of the point scatterer velocity is:

$$v_s(t) = \omega_R r_p \sin(\omega_R t)$$

where $r_p = \sqrt{x_p^2 + y_p^2}$. Obviously, from the same figure we have:

$$\begin{aligned} y_p &= r_p\sin(\omega_R t) \\ x_p &= r_p\cos(\omega_R t). \end{aligned}$$

Thus, for the interval $[t, t + \Delta t]$, the cross-range coordinate moves within:

$$[y_p, y_p + \Delta y_p] = [r_p\sin(\omega_R t), r_p\sin(\omega_R(t + \Delta t))]$$

where

$$\begin{aligned} y_p + \Delta y_p &= r_p\sin(\omega_R(t + \Delta t)) \\ &= r_p\sin(\omega_R t)\cos(\omega_R\Delta t) + r_p\cos(\omega_R t)\sin(\omega_R\Delta t) \\ &= y_p\cos(\omega_R\Delta t) + x_p\sin(\omega_R\Delta t). \end{aligned}$$

For small $\omega_R \Delta t$ we can write:

$$\begin{aligned} y_p + \Delta y_p &\cong y_p + x_p \omega_R \Delta t - y_p \frac{(\omega_R \Delta t)^2}{2} - x_p \frac{(\omega_R \Delta t)^3}{6} + ... \\ &\cong y_p + x_p \omega_R \Delta t. \end{aligned} \tag{5}$$

Then, the LOS projection of the velocity changes within

$$[v_s(t), v_s(t) + \Delta v_s(t)] = [\omega_R y_p, \omega_R y_p + x_p \omega_R \Delta t] \tag{6}$$

meaning that for intervals, such that $x_p \omega_R \Delta t$ can not be neglected with respect to y_p, the Doppler shift is a linear function of time with rate $x_p \omega_R$. Thus, instead of the delta pulse concentrated at one frequency, corresponding to $\omega_R y_p$ we will obtain a function corresponding to a LFM (Linear Frequency Modulation) signal whose instantaneous frequency changes according to Equation (6). The same holds for the range coordinate x_p.

If the assumption about small enough $\omega_R \Delta t$ does not hold then the changes of instantaneous frequency are not linear. In addition, if ω_R is not constant, then high nonlinearity in the instantaneous frequency can be expected, (5). The result is that, instead of having a 2D Fourier transform concentrated at the point corresponding to (x_p, y_p), we will obtain a spread Fourier transform, meaning a blurred radar image.

4 Fourier transform in ISAR

The two-dimensional (2D) Fourier transform of the received signal is:

$$Q(m',n') = \sum_{m=0}^{M-1}\sum_{n=0}^{N-1} q(m,n)\exp(-j[2\pi mm'/M + 2\pi nn'/N])$$

where time is discretized such that $t - mT_r = nT_s$. The periodogram:

$$P(m',n') = |Q(m',n')|^2$$

represents an ISAR image.

In order to analyze cross-range nonstationarities in the Fourier transform, we consider only the Doppler component part of the received signal (the p-th point scatterer), as it is usually done in the literature on ISAR:

$$\begin{aligned} e_p(t) &= \sigma_p \exp(j\frac{2\omega_0}{c}d_p(t)) \\ &= \sigma_p \exp(j\frac{2\omega_0}{c}(x_p\cos(\theta_R(t)) + y_p\sin(\theta_R(t)). \end{aligned} \tag{7}$$

The Fourier transform of $e_p(t)$ produces:

$$E_p(\omega) = \int_{-Tc/2}^{T_c/2} e_p(t)\exp(-j\omega t)dt = \int_{-\infty}^{\infty} w(t)e_p(t)\exp(-j\omega t)dt,$$

where $w(t)$ is the window defining the considered time interval (CIT). In order to simplify the notation we will just omit the index p.

For time-varying $d(t)$, we can write a Taylor series expansion of $d(t)$ around $t = 0$:

$$\begin{aligned} d(t) &= d_0 + d'(0)t + \frac{1}{2}d''(0)t^2 + ... \\ &= \sum_{n=0}^{\infty}\frac{1}{n!}d^{(n)}(0)t^n, \end{aligned} \tag{8}$$

where $d^{(n)}(0)$ is the $n-$th derivative of the distance at $t = 0$ and $2\omega_0 d'(0)/c = \Delta\omega_d$.

Fourier transform of (7) with (8) is of the form:

$$\begin{aligned} E(\omega) &= \int_{-\infty}^{\infty} w(t)\exp(j\frac{2\omega_0}{c}\sum_{n=0}^{\infty}\frac{1}{n!}d^{(n)}(0)t^n)\exp(-j\omega t)dt \\ &= \int_{-\infty}^{\infty} w(t)\exp(j\frac{2\omega_0}{c}\left\{[d(0) + d'(0)t + \sum_{n=2}^{\infty}\frac{1}{n!}d^{(n)}(0)t^n\right\})\exp(-j\omega t)dt. \end{aligned} \tag{9}$$

Now, by omitting the constant term $d(0)$ and shifting $2\omega_0 d'(0)/c = \Delta\omega_d$ into the second exponential term we get:

$$E(\omega) = \int_{-\infty}^{\infty} w(t) \exp(j\frac{2\omega_0}{c} \sum_{n=2}^{\infty} \frac{1}{n!} d^{(n)}(0) t^n) \exp(-j[\omega - 2\omega_0 d'(0)/c]t) dt. \qquad (10)$$

This is a Fourier transform of a product of the window $w(t)$ and the first exponential function, calculated at the frequency $\omega - 2\omega_0 d'(0)/c = \omega - \Delta\omega_d$. The Fourier transform of a product of two functions is equal to the convolution of their Fourier transforms, resulting in:

$$E(\omega) = W(\omega - \Delta\omega_d) *_\omega FT \left[\exp(j\frac{2\omega_0}{c} \sum_{n=2}^{\infty} \frac{1}{n!} d^{(n)}(0) t^n) \right],$$

where $*_\omega$ denotes convolution in frequency. Thus, the Fourier transform is located at and around the Doppler shift $\omega = \Delta\omega_d$. It is spread by the factor:

$$S_{spread}(\omega) = FT \left[\exp(j\frac{2\omega_0}{c} \sum_{n=2}^{\infty} \frac{1}{n!} d^{(n)}(0) t^n) \right].$$

This factor depends on the derivatives of the distance, starting from the second order (first order derivative of the Doppler shift), i.e., the spread factor depends on:

$$s_f(t) = \frac{1}{2} d''(0) t^2 + \frac{1}{6} d'''(0) t^3 + ...$$

It can significantly degrade the periodogram image:

$$P(\omega) = |E(\omega)|^2.$$

5 S-method-based improvement of the radar image

In this section, we will present a method for improvement of images blurred due to the long CIT and/or nonuniform movement. Instead of using the Fourier transform (periodogram), we use the S-method defined by [51]:

$$SM(\omega) = \frac{1}{\pi}\int_{-\infty}^{\infty} E(\omega+\theta)E^*(\omega-\theta)d\theta. \tag{11}$$

This method can improve the image concentration in a numerically very simple and efficient way. Namely, by replacing $E(\omega)$ from (9) into (11) we get:

$$\begin{aligned} SM(\omega) &= \frac{1}{\pi}\int_{-\infty}^{\infty}\int_{-\infty}^{\infty}\int_{-\infty}^{\infty} w(t_1)w^*(t_2) \\ &\quad \times \exp(j\frac{2\omega_0}{c}\sum_{n=0}^{\infty}\frac{1}{n!}d^{(n)}(0)t_1^n)\exp(-j\frac{2\omega_0}{c}\sum_{n=0}^{\infty}\frac{1}{n!}d^{(n)}(0)t_2^n) \\ &\quad \times \exp(-j(\omega+\theta)t_1)\exp(j(\omega-\theta)t_2)dt_1dt_2d\theta. \end{aligned}$$

The part of integrand depending on θ is $\exp(-j\theta(t_1+t_2))$. Integration over θ results in $2\pi\delta(t_1+t_2)$. Integration of a function $g(t_1)g(t_2)\delta(t_1+t_2)$ over t_1 results in the function $g(t)g(-t)$ for $t_1=-t_2=t$. From the previous equation it means that we obtain:

$$\begin{aligned} SM(\omega) &= 2\int_{-\infty}^{\infty} w(t)w^*(-t) \\ &\quad \times \exp(j\frac{2\omega_0}{c}\sum_{n=0}^{\infty}\frac{1}{n!}d^{(n)}(0)(t^n-(-t)^n)\exp(-j2\omega t)dt \\ &= W_e(\omega-\Delta\omega_d) *_\omega FT\left[\exp(j\frac{2\omega_0}{c}(\frac{1}{3!}d^{'''}(0)t^3+...\right] \end{aligned}$$

where similar calculations as in (9)-(10) are performed.

The S-method-based image is located at the same position in Doppler space as the Fourier transform image, $\omega=\Delta\omega_d$, but with the spreading term:

$$S_{spread}(\omega) = FT\left[\exp(j\frac{2\omega_0}{c}(\frac{1}{3!}d^{'''}(0)t^3+...\right].$$

Its exponent starts from the third derivative $d^{'''}(0)$:

$$s_f(t) = \frac{1}{6}d'''(0)t^3 + \frac{1}{120}d^{(5)}(0)t^5 + ...$$

This means that the S-method has the ability to automatically compensate for quadratic and all even higher-order terms in phase. Recall that in the Fourier transform based image the spreading terms started from the second derivative $d^{''}(0)$. It means that in the S-method, the points with linear Doppler changes:

$$\frac{2\omega_0}{c}d'(t) = \Delta\omega_d(t) = \Delta\omega_d + at$$

will be fully concentrated without any spread, since here $s_f(t) = 0$. Thus, targets with constant acceleration will undergo full motion compensation and their point-scatterers will each be localized. Note that $W_e(\omega)$ is the Fourier transform of window $w(t/2)w^*(-t/2)$ while $\Delta\omega_d$ without argument denotes the constant part of $\Delta\omega_d(t)$, i.e., $\Delta\omega_d = \Delta\omega_d(0)$. It should also be noted that the source of the quadratic term can come from not only acceleration, but also can come from non-uniform rotational motion and the cosine term in wide-angle imaging.

5.1 Numerical implementation

The discrete version of (11) is:

$$\begin{aligned} SM(k) &= \sum_{l=-L}^{L} E(m+l)E^*(m-l) \\ &= |E(m)|^2 + 2\,\mathrm{real}\{\sum_{l=1}^{L} E(m+l)E^*(m-l)\}. \end{aligned}$$

In theory, L should be such as to provide calculation over the whole frequency range. However since the first term is $|E(l)|^2$, i.e., the periodogram, while the terms $2\,\mathrm{real}\{E(m+l)E^*(m-l)\}$, for $l = 1, 2, ...$, are used to improve the periodogram concentration in the case of time-varying Doppler shift, only a few terms are enough to provide complete integration over one target point and achieve high resolution. The S-method can be realized in a recursive form, as well. If we denote:

$$SM_L(m) = \sum_{l=-L}^{L} E(m+l)E^*(m-l)$$

then

$$SM_L(m) = SM_{L-1}(m) + 2\,\mathrm{real}\{E(m+L)E^*(m-L)\}, \tag{12}$$

with $SM_0(m) = |E(m)|^2$ being the standard Fourier transform based representation.

Therefore, the S-method improvement can be achieved starting with the radar image, with additional simple matrix calculation according to (12). It is obvious that the total calculation complexity, for adding one more term to the existing Fourier

transform image or to the existing S-method image, is one addition and one multiplication, for each point. For each next $L+1$, just one more multiplication and addition is needed. In theory, when L is equal to the width of the auto-term (width of the blurred point in the radar image) the radar image is completely focused and there is no need to further increase L. In practice, it means just to take two to six terms for L. Note that it is also possible to use S-method with self-adaptive number of samples. A very detailed analysis of calculation complexity may be also found in [51]. A detailed description of the S-method and its application to simulated and measured data can be found in [**?**, 16–19, 22, 39, 48–50, 57–61].

The radar image can be obtained by using the 2D FT as:

$$Q(m',n') = \sum_{m=0}^{M-1}\sum_{n=0}^{N-1} w(m)q(m,n)\exp(-j[2\pi mm'/M + 2\pi nn'/N]).$$

where $w(m)$ is a window function used to reduce spectral leakage effects in the FT domain.

As described in the previous section, the S-method (SM) can be defined for radar images as:

$$SM_1(m',n') = \sum_l \Pi(l)Q(m'+l,n')Q^*(m'-l,n'), \tag{13}$$

where $\Pi(l)$ is a window in the frequency domain. For fixed n' this form is the 1D SM for fixed range cell. In similar manner, the radar image based on the 1D SM for fixed cross-range cell is:

$$SM_2(m',n') = \sum_i \Pi(l)Q(m',n'+i)Q^*(m',n'-i). \tag{14}$$

Also, the 2D SM is:

$$SM_3(m',n') = \sum_l\sum_i \Pi(l,i)Q(m'+l,n'+i)Q^*(m'-l,n'-i). \tag{15}$$

Commonly, the frequency window function is rectangular, and for 1D SM given with (13) exhibits:

$$\Pi(l) = \begin{cases} 1 & |l| \le L \\ 0 & \text{elsewhere.} \end{cases} \tag{16}$$

Then, the corresponding SM form can be calculated as:

$$SM_1(m',n') = |Q(m',n')|^2 + 2\,\mathrm{Re}\left\{\sum_{l=1}^{L} Q(m'+l,n')Q^*(m'-l,n')\right\}. \tag{17}$$

For $L = 0$ we obtain the standard radar image (defocused but without spurious terms), while for large L the radar image approaches the WD-based image (focused but with interfering cross-terms). Fortunately, for relatively small L the radar image could be significantly improved without introducing the interference. A drawback of this technique is demonstrated in the next subsection on a simple example.

5.2 Illustrative example

Consider three point targets. The first and third targets are moving with constant velocity in SAR (equivalent to the uniform acceleration in ISAR), while the second is non-moving target in SAR (equivalent to the constant velocity in ISAR). The returned radar signal from these three targets can be modelled as (Sections 2 and 3):

$$x(n) = A(n)e^{-j\frac{0.4}{256}\pi n^2}e^{-j\frac{\pi}{2}n} + A(n)e^{j\frac{\pi}{8}n} + A(n)e^{j\frac{0.2}{256}\pi n^2}e^{j\frac{\pi}{3}n},$$

where the amplitude $A(n)$ is slow-varying, defined as $A(n) = \frac{1}{2} + \frac{1}{2}\cos\frac{2\pi}{256}n$. The signal is observed for $-128 \leq n \leq 127$. For the considered time instant $n = 0$, it will be: $\omega_1(0) = -\frac{\pi}{2}$, $\omega_2(0) = \frac{\pi}{8}$ and $\omega_3(0) = \frac{\pi}{3}$.

The spectrogram of the analyzed signal is shown in Figure 2a. The first and third targets are spread and not visible compared to the second target. Note that the radar signal returned from the second target is constant frequency component, while the radar signals returned for the first and third targets are linear FM. The spectrogram corresponds to the SM with $L = 0$. By increasing the value of L, $L = 4$, the concentration of the first and third targets is improved, Figure 2b, but these targets are still spread compared to the second one. For higher value of L, $L = 16$, the concentration of the components continue to increase, but the cross-term appears between close targets, the second and third in Figure 2c. The desired concentration of the first and third components is achieved by using the SM with L equal to the signal length, but this value generates very strong cross-terms between components, Figure 2d. The cross-term between the second and third component is almost strong as useful components. Thus, it is clear that we need a more sophisticated technique for radar imaging in order to achieve high concentration without interferences. Fortunately, one possible solution, the adaptive SM, is quite simple. The resulting representation of the analyzed signal is given in Figure 2e. Here, we assumed that the value of L depends on the considered frequency. It can be observed that high values of L are used where concentration improvement is necessary (around $\omega_1(0)$ and $\omega_3(0)$), while in the case when the component is well concentrated in the spectrogram, very low values of L (or $L = 0$) are used. In the next section, the selection of the adaptive window in real problems is discussed.

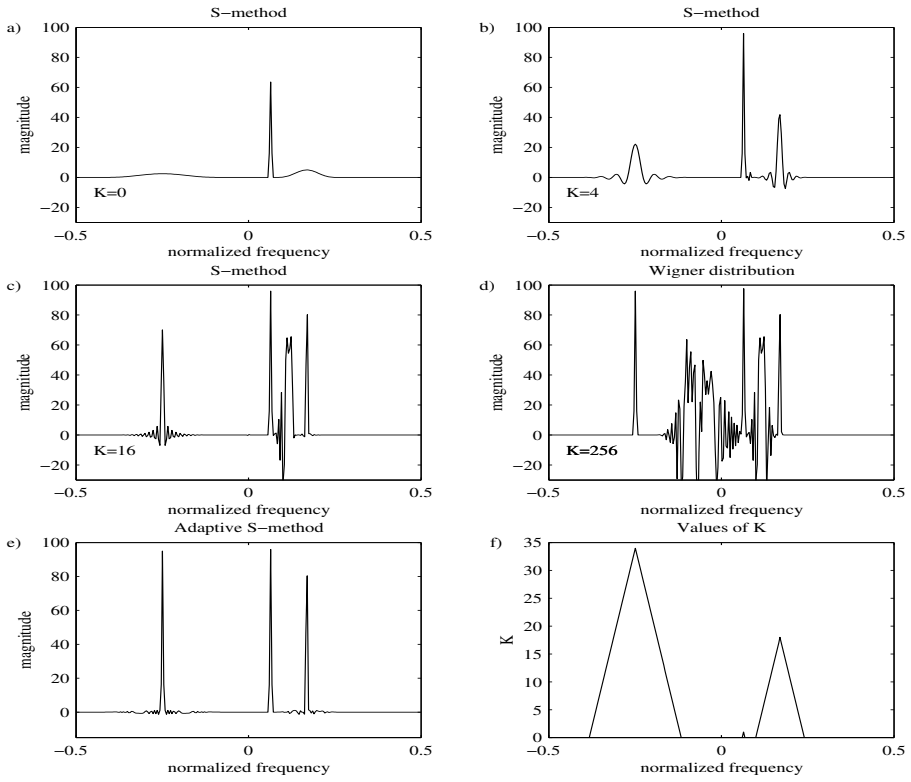

Figure 2: *Representation of the three-component signal by using: a) spectrogram (S-method with $L = 0$), b) S-method with $L = 4$, c) S-method with $L = 16$, d) Wigner distribution (S-method with L equal to the signal length) and e) adaptive S-method. f) Values of L used for obtaining the adaptive S-method.*

6 Adaptive S-method-based radar image

6.1 Adaptive 1D SM

Here, we give a form of the adaptive SM for fixed range cell, but in the same manner it can be evaluated for fixed cross-range cell. The adaptive SM is originally developed for improving the TF representation in [52]. The adaptive 1D SM for radar images can be defined as:

$$SM_1(m',n') = |Q(m',n')|^2 + 2\,\mathrm{Re}\left\{ \sum_{l=1}^{L(m',n')} Q(m'+l,n')Q^*(m'-l,n') \right\}. \qquad (18)$$

The main problem here is the determination of $L(m',n')$. $L(m',n')$ can simply be obtained as a maximal value of l for which the term $\mathrm{Re}\{Q(m'+l,n')Q^*(m'-l,n')\}$ used for the SM calculation is greater than a specific threshold $R(m',n')$, and where all $\mathrm{Re}\{Q(m'+l',n')Q^*(m'-l',n')\}$ for $|l'| < |l|$ are greater than the threshold. This can be written as:

$$L(m',n') = \arg\max_{l} \bigwedge_{l'=1}^{l} \left(\mathrm{Re}\{Q(m'+l',n')Q^*(m'-l',n')\} \geq R(m',n')\right), \qquad (19)$$

where $\bigwedge_{l'=1}^{l}$ represents logical operation and applied to logical expressions from argument for various $l' = 1, ..., l$. The threshold value can be determined in various ways. The global threshold is proposed in [52] as:

$$R = \varepsilon \max_{m',n'} |Q(m',n')|^2, \qquad (20)$$

where ε can be adopted as a small value, for example $\varepsilon \in [0.1\%, 5\%]$. Of course, this threshold can be calculated in the same manner for considered range or cross-range cell. In this way, components having small energy are removed and they are indication of the end of the useful radar component. In the case of images corrupted by noise, we can select global threshold as:

$$R = \max\left\{ \varepsilon \max_{m',n'} |Q(m',n')|^2, \kappa^2\sigma^2(m',n') \right\}, \qquad (21)$$

where $\sigma^2(m',n')$ is variance of the radar image caused by the noise. An analysis of noise in the SM can be found in [53]. In this case, we can remove all weak components, as well as the components influenced by noise. Parameter κ is commonly selected to be around $\kappa = 3$ (three sigma rule).

This thresholding approach can be applied locally for regions of the radar image. In addition, well-described techniques from the digital image processing can be used

in this application [54]. The procedure for the threshold determination based on the Otsu algorithm is used here [54]. The 2D FT magnitude $|Q(m', n')|$ is taken as image pixels intensity needed for the algorithm The procedure for the threshold determination based on the Otsu algorithm is summarized as:

Step 1 Estimate the initial value for threshold. Here, the initial value for threshold is set to the half of the pixels intensity maximum:

$$\rho = \frac{1}{2} \max_{m',n'} |Q(m', n')|. \tag{22}$$

Step 2 Calculate two sums S_1 and S_2, where S_1 is a sum of intensity values of the pixels whose intensity is larger than the current threshold ρ:

$$S_1 = \sum_{m',n'} |Q(m', n')| \quad (\forall\,(m', n')\,,\ |Q(m', n')| > \rho) \tag{23}$$

while, S_2 is a sum of intensity values of the pixels whose intensity is smaller than the current threshold ρ:

$$S_2 = \sum_{m',n'} |Q(m', n')| \quad (\forall\,(m', n')\,,\ |Q(m', n')| < \rho)\,. \tag{24}$$

Step 3 Calculate two new thresholds, ρ_1 and ρ_2, as average values of the obtained sums:

$$\rho_1 = \frac{S_1}{N_1},\ \rho_2 = \frac{S_2}{N_2}, \tag{25}$$

where N_1 and N_2 are number of elements summed in (23) and (24) respectively.

Step 4 Compute a new threshold value:

$$\rho = \frac{1}{2}(\rho_1 + \rho_2). \tag{26}$$

Step 5 Repeat steps 2 through 4 until the difference in ρ in successive iterations is smaller than a predefined parameter, or for a specified number of iteration.

The thresholds used in our simulations are obtained after five iterations. Its squared value, $R = \rho^2$, is used in both 1D and 2D adaptive SM calculation.

6.2 Adaptive 2D SM

The adaptive 2D SM can be evaluated as [42]:

$$SM_3(m',n') = |Q(m',n')|^2 + 2\,\mathrm{Re}\left\{\sum_{l=0}^{L(m',n')}\sum_{i=1}^{I(m',n')} Q(m'+l,n'+i)Q^*(m'-l,n'-i)\right\} + 2\,\mathrm{Re}\left\{\sum_{l=1}^{L(m',n')}\sum_{i=-I(m',n')}^{0} Q(m'+l,n'+i)Q^*(m'-l,n'-i)\right\}. \quad (27)$$

Here, we have to determine two adaptive values $L(m',n')$ and $I(m',n')$ for each pixel in the radar image. However, multiparameter optimization in this case is difficult and it could lead to non-optimal solutions. Instead, we will use $O(m',n') = L(m',n') = I(m',n')$, so just one adaptive value for width of the used square window has to be determined. The adaptive square window width $O(m',n') = O$ for the considered radar image pixel can be determined as a maximal value of O for which all terms $Q(m'+l,n'+i)Q^*(m'-l,n'-i)$ for $|l,i| \leq O$ (inside and at the border of the used square window) are greater than a specific threshold $R(m',n')$. This can be written as:

$$O(m',n') = \arg\max_{O} \bigwedge_{l,i=1}^{O} \left(Q(m'+l,n'+i)Q^*(m'-l,n'-i) \geq R(m',n')\right). \quad (28)$$

The adaptive 2D SM can improve concentration of the radar image using information from both the range and cross-range cells and it can be useful in the case of images with significant spreading in both directions. This spreading can occur in the case of very complicated maneuvers or in the case when radar and target are relatively close to each other, but also in some other setups.

Now, we overview all advantages of the proposed techniques. The adaptive SM is a postprocessing technique that modifies standard radar image calculated by using the 2D FT. Additional processing consists of two parts: threshold evaluation and adding terms to the standard radar image. Both these steps require just a moderate calculation burden, since they consist of simple multiplications, additions and logical operations. In addition, hardware realization of the SM is well developed for both 1D and 2D signals [62]. This hardware requires just a moderate modification to be used in the proposed application. As it will be seen from Section 4, achieved results with the SM are quite accurate and we see this approach as one of the main candidates to be used as a trade-off between accuracy and quality of radar images and computational demands.

A detailed description of the adaptive S-method and its application to simulated and measured data can be found in [17–19, 42, 46, 48–50].

7 Local polynomial Fourier transform-based radar image

There are signals whose form is known up to an unknown set of parameters. For example, many signals could be expressed as polynomial-phase signals [15, 24]:

$$x(t) = Ae^{j(\Omega_0 t + a_1 t^2 + a_2 t^3 + \cdots + a_N t^{N+1})}$$

where the parameters $\Omega_0, a_1, a_2, \ldots, a_N$ are unknown. A high concentration of such signals in the frequency domain is achieved by the polynomial Fourier transform defined by:

$$PFT_{\Omega_1,\Omega_2,\ldots,\Omega_N}(\Omega) = \int_{-\infty}^{\infty} x(t)e^{-j(\Omega t + \Omega_1 t^2 + \Omega_2 t^3 + \cdots + \Omega_N t^{N+1})}dt \tag{29}$$

when parameters $\Omega_1, \Omega_2, \ldots, \Omega_N$ are equal to the signal parameters $a_1, a_2, \ldots, a_N$. Finding values of unknown parameters $\Omega_1, \Omega_2, \ldots, \Omega_N$ that match signal parameters can be done by a simple search over a possible set of values for $\Omega_1, \Omega_2, \ldots, \Omega_N$ and stopping the search when the maximally concentrated distribution is achieved (in an ideal case, the delta function at $\Omega = \Omega_0$, for $\Omega_1 = a_1$, $\Omega_2 = a_2$, ... is obtained). This procedure may be time-consuming.

For non-stationary signals, this approach may be used if the nonstationary signal could be considered as a polynomial phase signal within the analysis window. In that case, the local polynomial Fourier transform (LPFT), proposed by Katkovnik [55,56], may be used. It is defined as:

$$LPFT_{\Omega_1,\Omega_2,\ldots,\Omega_N}(t,\Omega) = \int_{-\infty}^{\infty} x(t+\tau)w(\tau)e^{-j(\Omega\tau + \Omega_1\tau^2 + \Omega_2\tau^3 + \cdots + \Omega_N\tau^{N+1})}d\tau. \tag{30}$$

In general, parameters $\Omega_1, \Omega_2, \ldots, \Omega_N$ could be time dependent, that is, for each time instant t, the set of optimal parameters could be different.

A detailed description of the local polynomial Fourier transform and its application to simulated and measured data can be found in [24, 41, 43, 47, 50].

8 SAR/ISAR toolbox

The SAR/ISAR toolbox was developed based on the algorithms described in the previous sections. Two approaches are implemented:

- S-method-based focusing
- Local polynomial Fourier transform (LPFT)-based focusing

Beside the core functions for the image focussing, the toolbox contains Virtual Instrument, Demo and Advanced Visualization capabilities.

8.1 Files and installation

The toolbox has five program files:

SM_ISAR.m This file performs S-method-based focusing of a given radar data. For more details, type `help SM_ISAR` in the MATLAB command line.

LPFT_ISAR.m This file performs the LPFT-based focusing of a given radar data. For more details, type `help LPFT_ISAR` in the MATLAB command line.

ISAR_VI.m This file is a Virtual Instrument, which is capable to perform focussing methods on user defined or simulated data. To start Virtual Instrument, type `ISAR_VI` in the MATLAB command line.

ISAR_demo.m This file is a demonstration of core functions' usage. To start demo, type `ISAR_demo` in the MATLAB command line.

ShowData.m This file is a function for advanced data visualization. It is used by Virtual Instrument and demo. This function can independently be used from the rest of the toolbox in order to visualize the arbitrary 2D data. The function is shared with the Time-Frequency toolbox. Two simulated data files are commonly used for testing the image focussing methods.

mig25.mat Mig data - The model is a MiG-25 aircraft with 120 point-scatterers distributed along the edge of the 2D shape of the aircraft. The simulation uses a stepped frequency X-band radar operating at a center frequency of 9 GHz. With a total of 64 stepped frequencies, it has a bandwidth of 512 MHz and a range resolution of 0.293 m. The PRF is 20 kHz and the CIT is 1.64 seconds. A total of 64 range cells and 512 cross-range cells are used for the imaging.

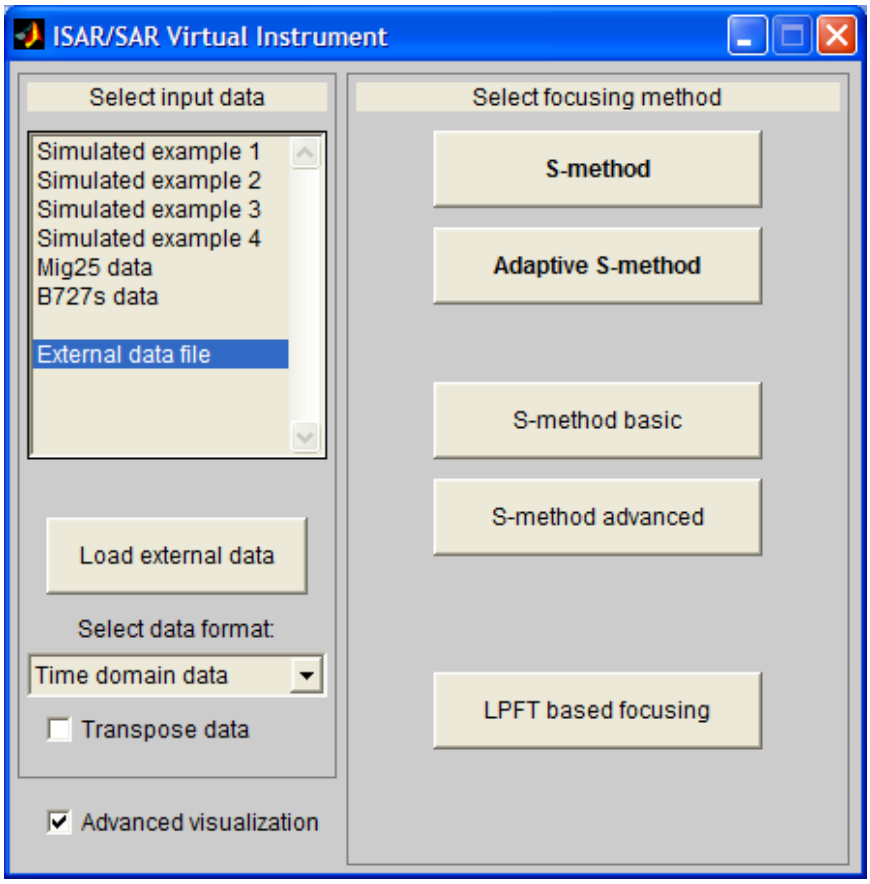

Figure 3: *Virtual instrument – main screen.*

B727S.mat Boeing data - The model is a Boeing 727 aircraft. The simulation uses a stepped frequency X-band radar operating at a center frequency of 9 GHz. With a total of 64 stepped frequencies, the waveform has a bandwidth of 150 MHz and a range resolution of 1 m. The PRF is 20 kHz and the CIT is 0.82 seconds. A total of 64 range cells and 256 cross-range cells are used in the imaging.

To install the toolbox, copy all the files in the working directory.

8.2 Virtual instrument

The Virtual Instrument is started with the command `ISAR_VI`. The main screen is presented in Figure 3. Other Virtual Instrument screens are presented in Figure 4, Figure 5 and Figure 6. The resulting image for Mig25 data is presented in Figure 7.

8.3 Main screen

The main screen is divided into two parts: signal definition part (left) and focussing part (right). Within the signal definition part, the user can select one of the predefined examples or external data file.

If the external data file is selected, the user can select the appropriate data format and choose to transpose data. The button “Load external data” is used to load the data from the file according to the selected format. It is assumed that the file is MATLAB MAT file with data stored in variable named q. If such variable is not found, the user is prompted to select the variable that contains data. After selecting the input data, the radar image is displayed.

Within the focusing part, the user can select S-method or adaptive S-method in order to obtain the focused image. In these cases, the image is focussed. Alternatively, by selecting the "S-method basic", "S-method advanced" or "LPFT-based focusing" (see Figure 3), the advanced focusing techniques are invoked. In these cases, the user can choose the required parameters to obtain the focused image. In these options, the user can explore and compare the results using different choice of parameters.

The user can enable or disable the advanced visualization options. When the advanced visualization is unchecked, the basic imagesc command is used to display the results.

8.4 S-method basic

Here, the user can choose to invoke S-method with constant L or adaptive S-method for a given threshold level Q (see Figure 4).

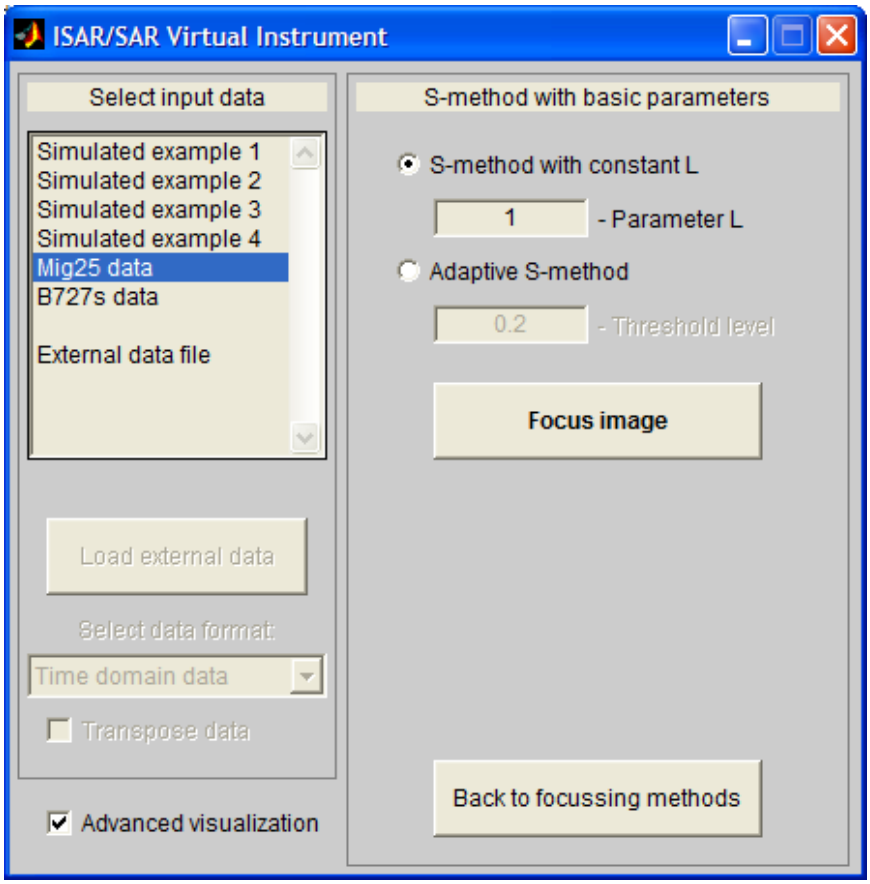

Figure 4: *Virtual instrument – S-method with basic options.*

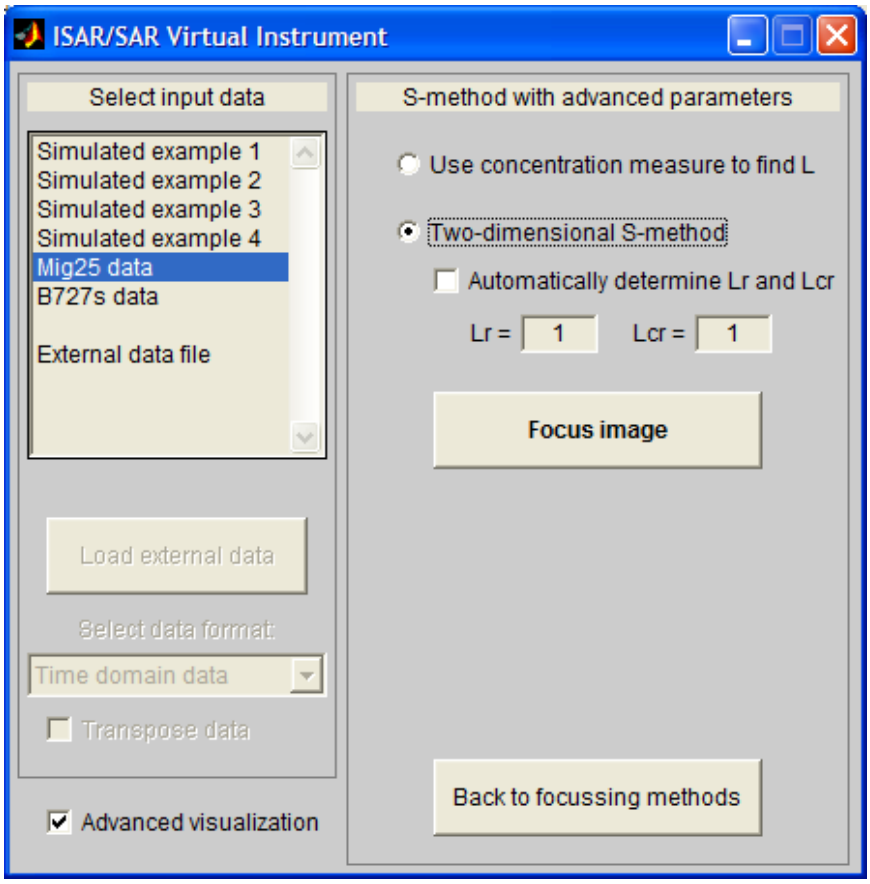

Figure 5: *Virtual instrument – S-method with advanced options.*

8.5 Advanced S-method

Two advanced techniques are given here (see Figure 5):

- S-method with L chosen in order to achieve the best concentration of the resulting image according to appropriate concentration measure. When the image is already focused along the range, the user can select this option to focus the target image. In this method, the concentration measure is used to determine L automatically.
- Two dimensional S-method, where the user can choose to calculate L_r and L_cr automatically or to enter desired values. When the image is not focused in both range and cross-range, the user can select this option to focus the target image. The user can explore and compare the results using different choice of parameters.

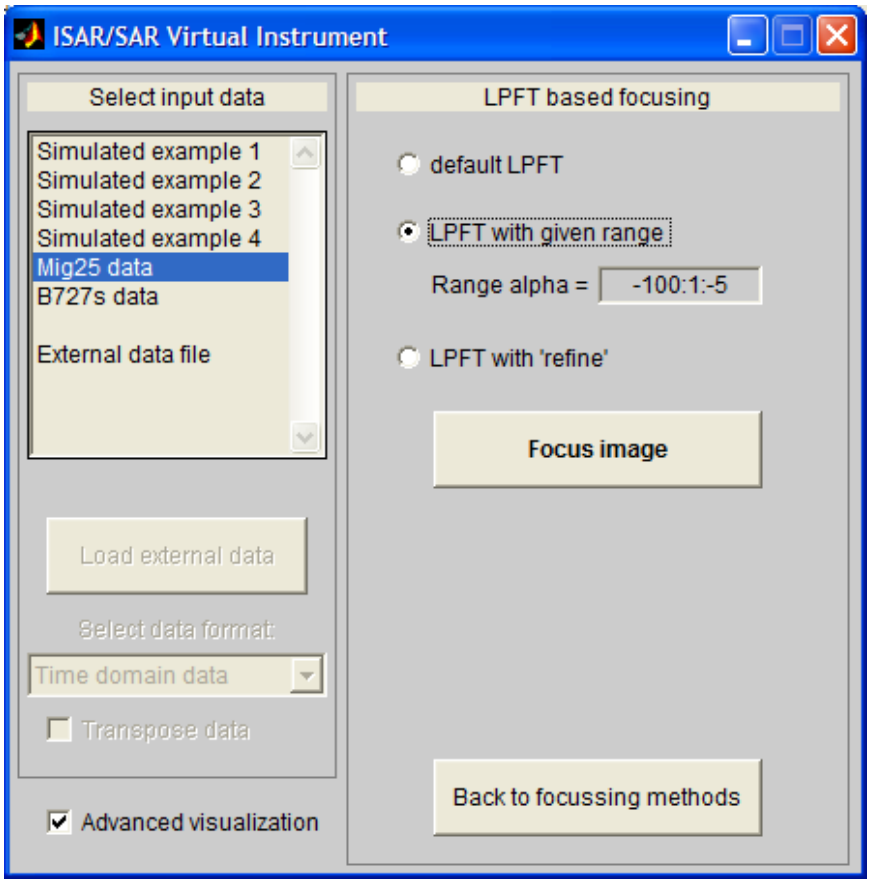

Figure 6: *Virtual instrument – LPFT-based focusing.*

8.6 LPFT-based focusing

For LPFT-based focusing, there are three options available (see Figure 6):

- LPFT with automatically chosen parameters
- LPFT with given range
- LPFT with "refine" option

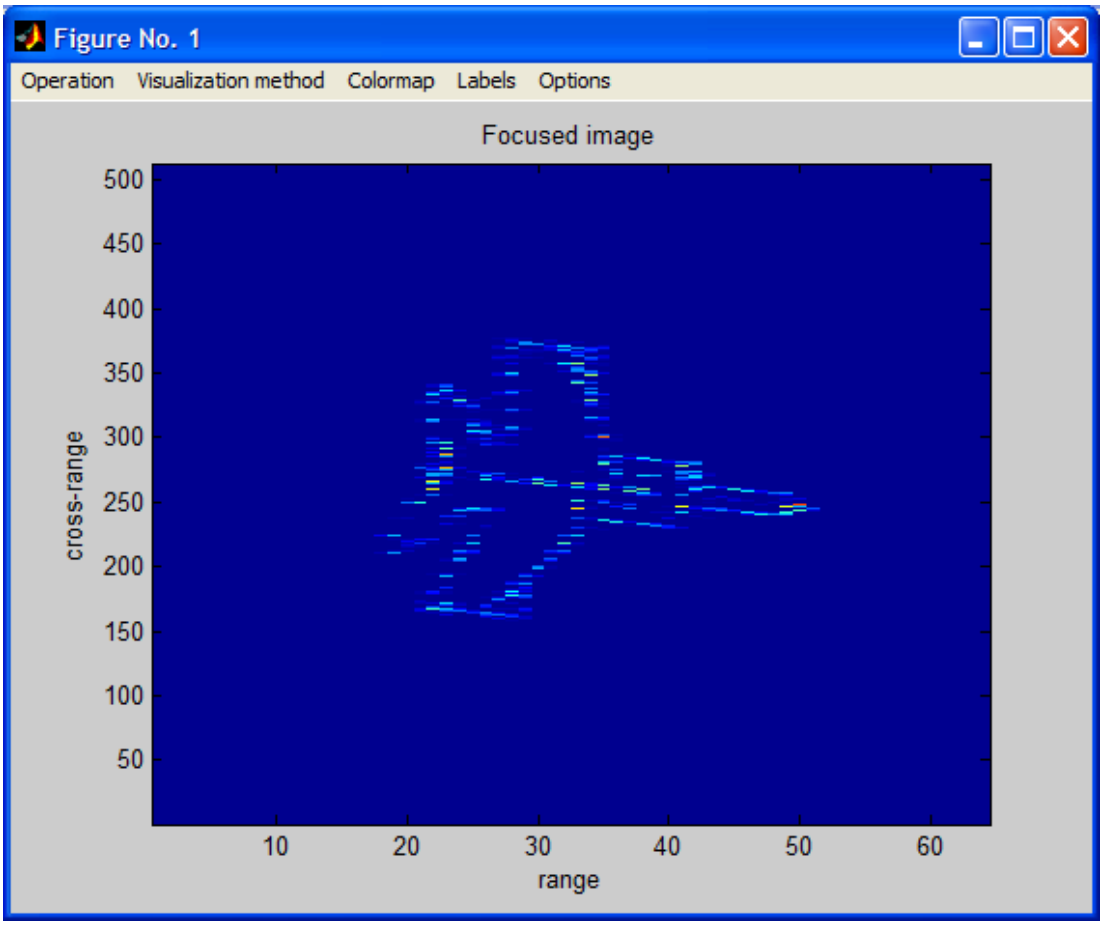

Figure 7: *Data visualization.*

8.7 Displaying results

When the user invoke "Focus image" command (see Figure 4, Figure 5 and Figure 6), the focused image is displayed. The example of the focused image in ISAR scenario is given in Figure 7. This result is obtained with advanced visualization option checked. For the comparison purpose, Figure 8 shows the original and focused image of the Mig-25 data. In this case, S-method is used to focus the target. Figure 9 shows the original and focused image of the B-727 data. The adaptive S-method is used to focus the target in this case. Figure 10 shows the original and focused image of the B-727 data. In this case, LPFT is used to focus the target. A more detailed description of these methods and comparison among these methods can be found in [14, 19, 22, 24, 36, 39, 41, 42, 59, 60]. In these studies, both simulation and measured data were used. The user can select various visualization options from the figure menus. These menus are described in the following section.

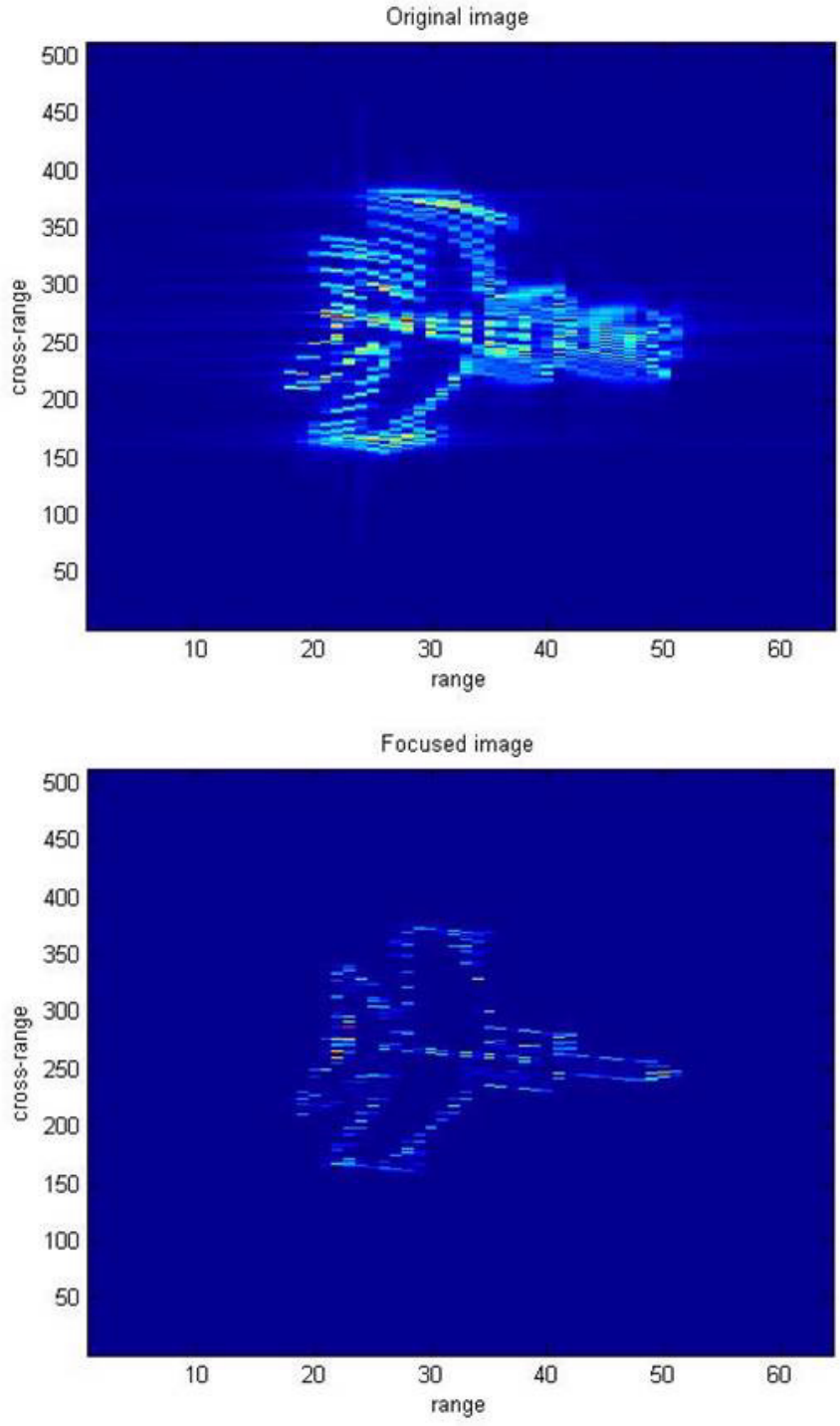

Figure 8: *Top - unfocused image using Fourier method; Bottom - focused image using S-method.*

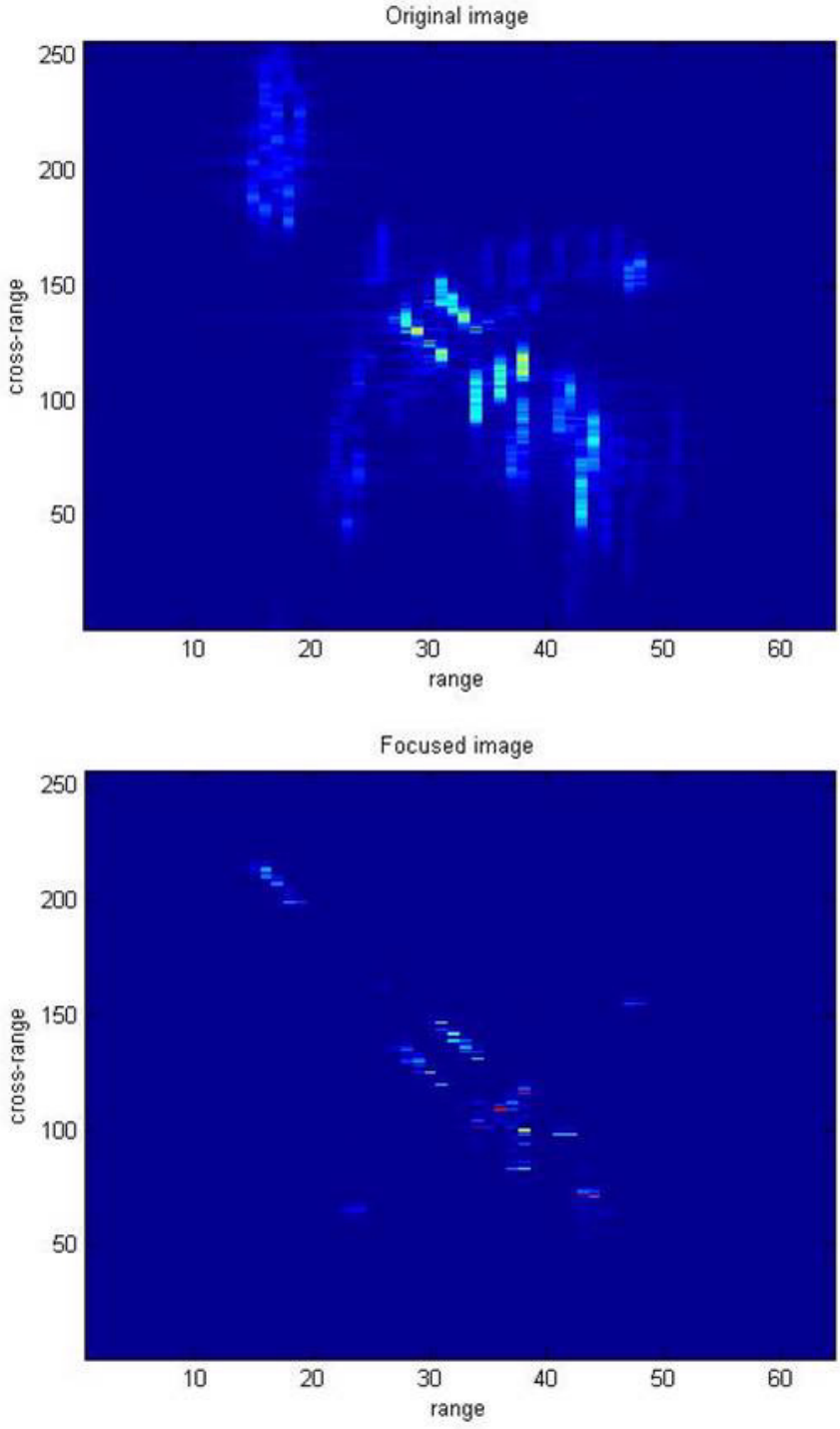

Figure 9: *Top - unfocused image using Fourier method; Bottom - focused image using adaptive S-method.*

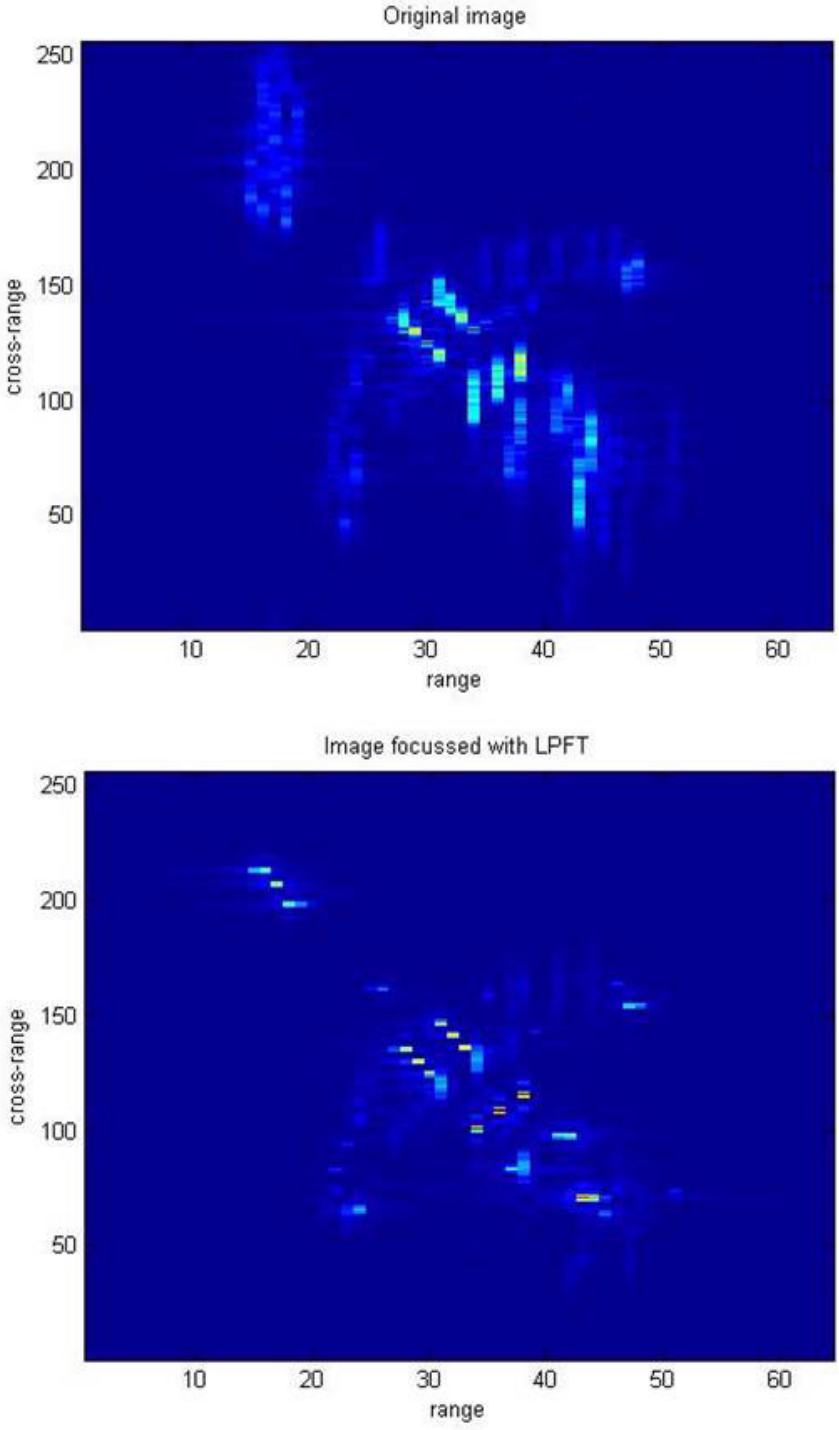

Figure 10: *Top - unfocused image using Fourier method; Bottom - focused image using LPFT method.*

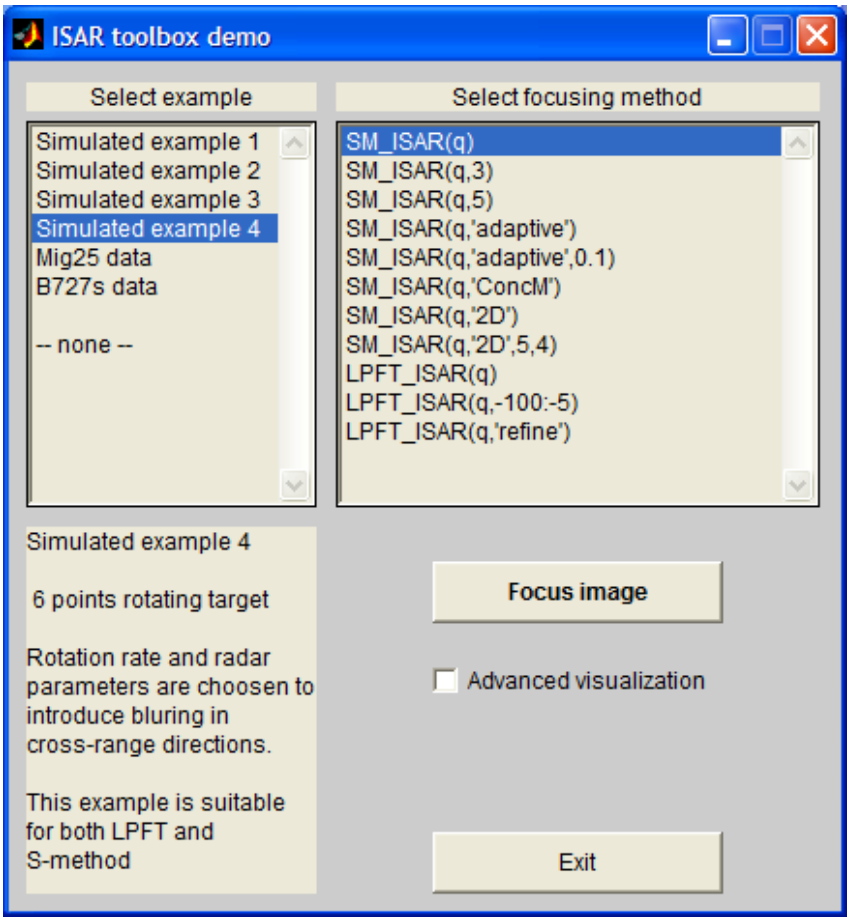

Figure 11: *ISAR toolbox demo.*

8.8 SAR/ISAR toolbox demo

The usage of the core functions, `SM_ISAR` and `LPFT_ISAR`, is explained in toolbox demo (see Figure 11). Type `ISAR_demo` in the MATLAB command line to start the demo.

The user can select the simulated input data and call the selected focusing function.

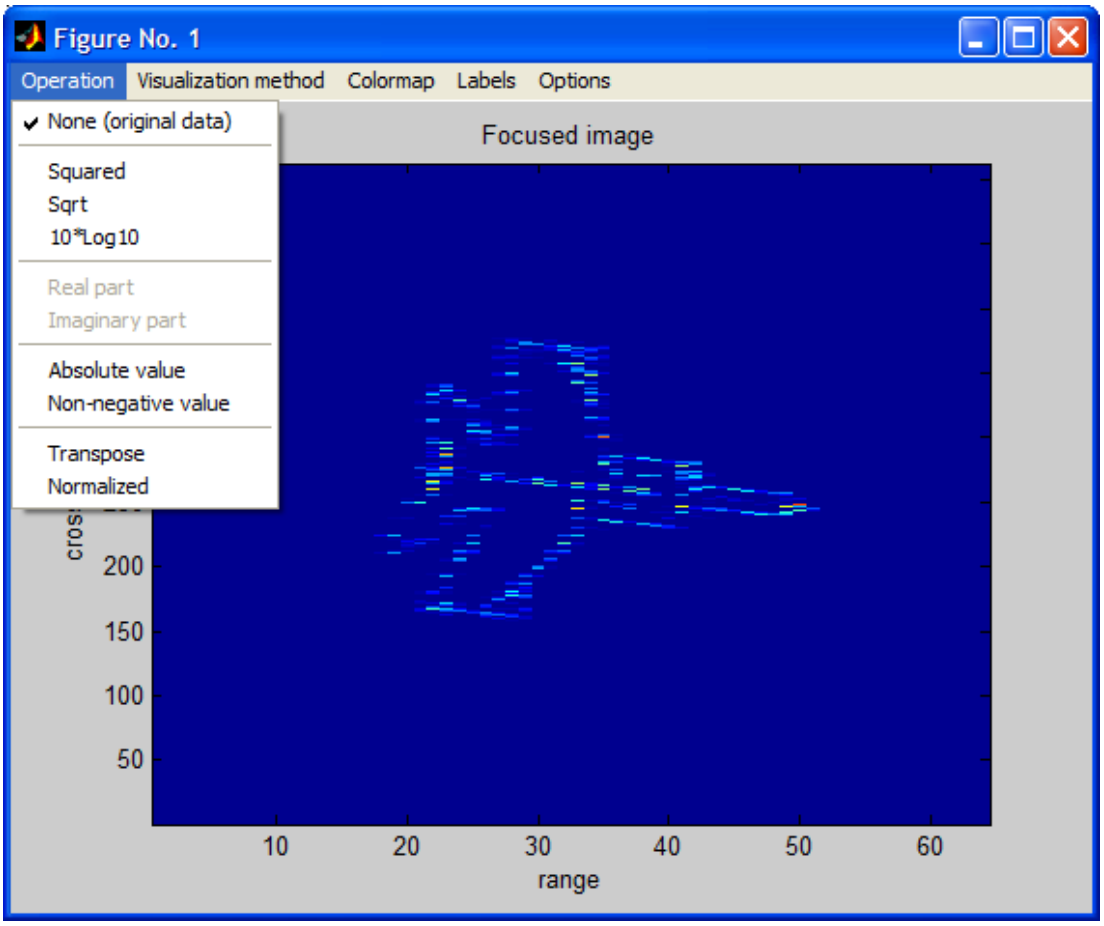

Figure 12: *Data visualization – operations menu.*

8.9 Advanced visualization

This operation menu (see Figure 12) allows the user to select the original data, squared data or square root of the data as well as the data in logarithmic scale. The user can also select the real or imaginary part in the case of displaying complex data as well as the absolute value or non-negative part. Moreover, the data can be transposed or normalized.

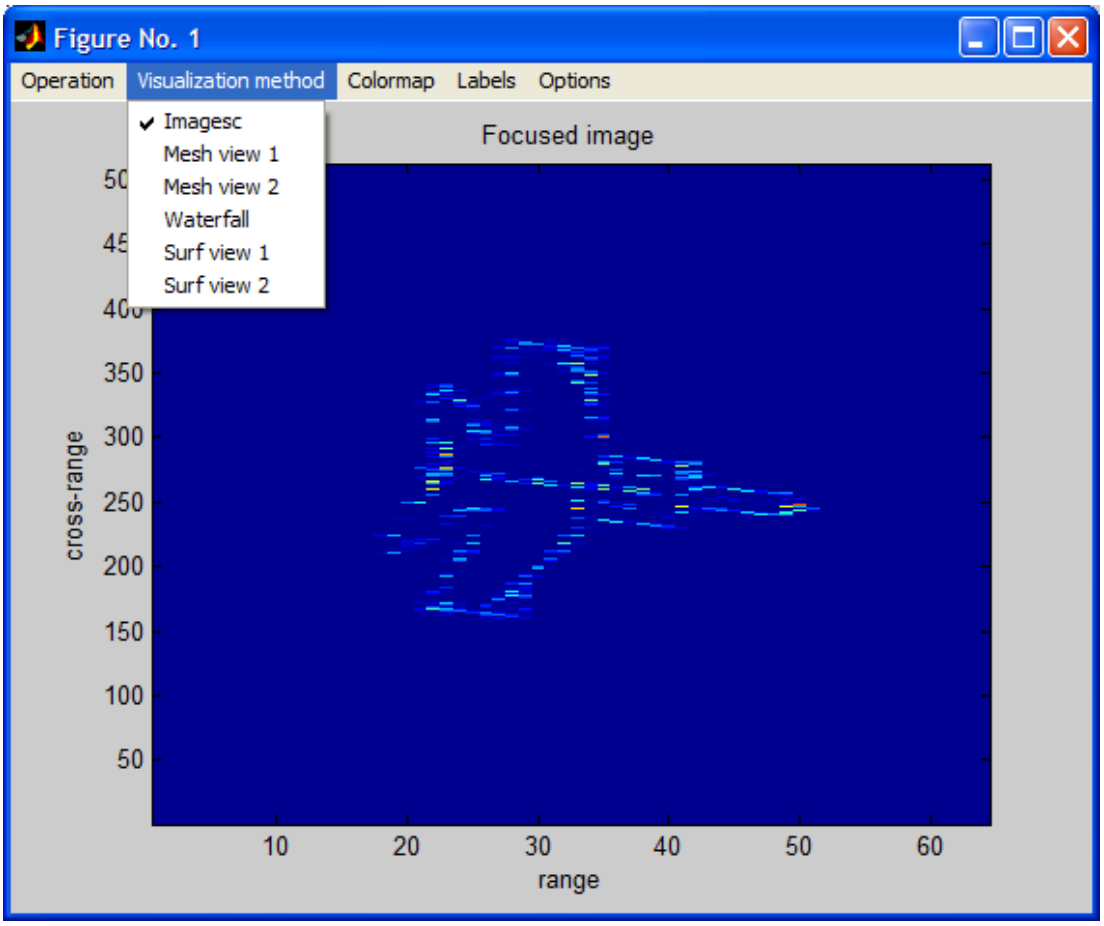

Figure 13: *Data visualization – operations menu.*

Six visualization methods are implemented (see Figure 13). Basic imagesc, two mesh types, waterfall and two surf types of visualizations are possible. These methods can be chosen from the "Visualization method" menu.

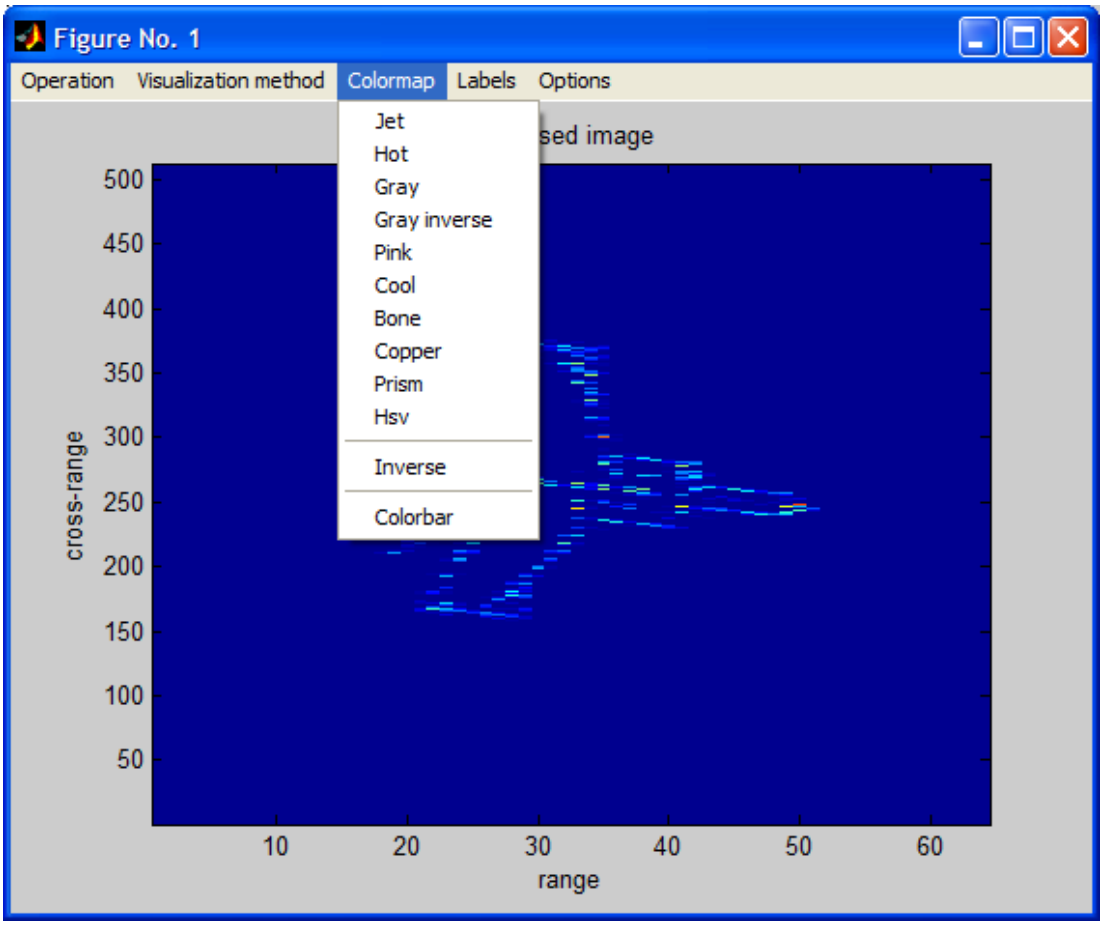

Figure 14: *Data visualization – operations menu.*

The "Colormap" menu (see Figure 14) allows user to select the appropriate colormap, or to show or hide the colorbar.

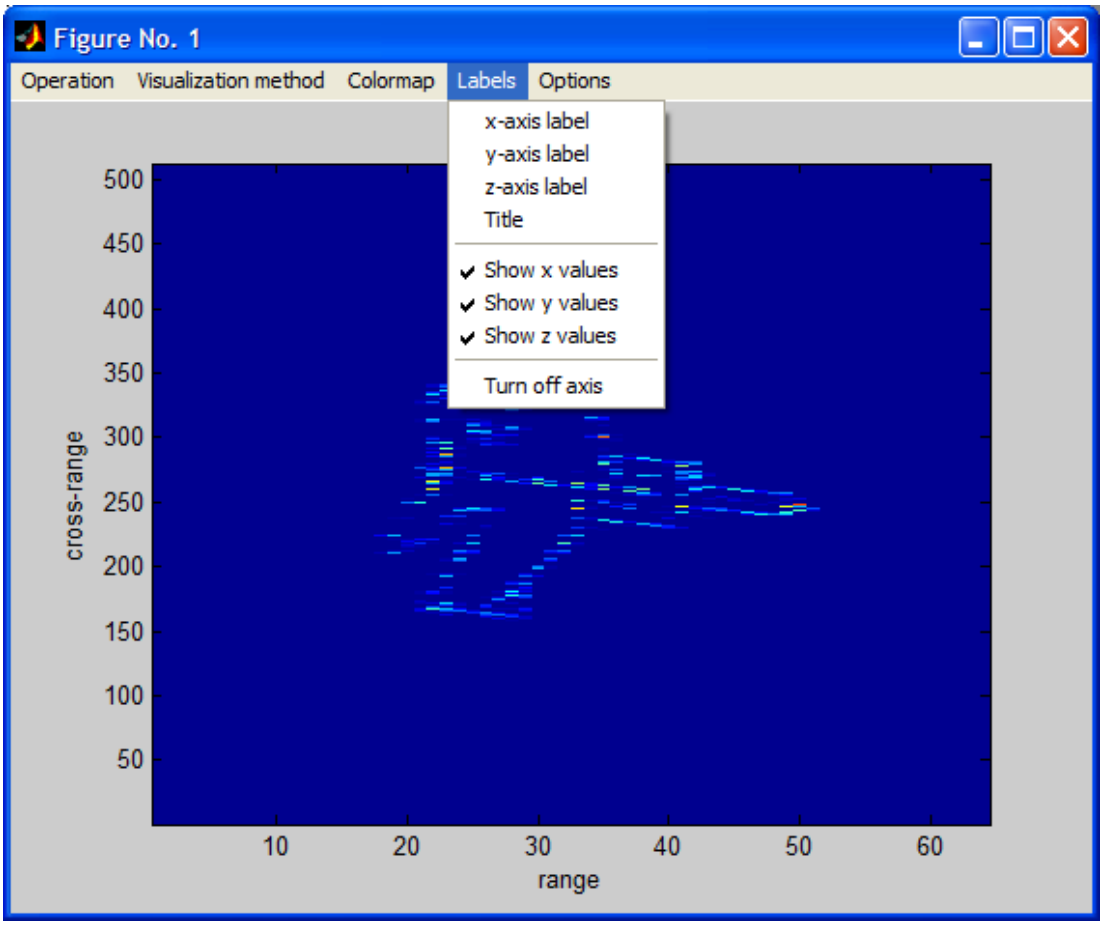

Figure 15: *Data visualization – operations menu.*

The "Labels" menu (see Figure 15) allows the user to use axis labels' definition and appearance.

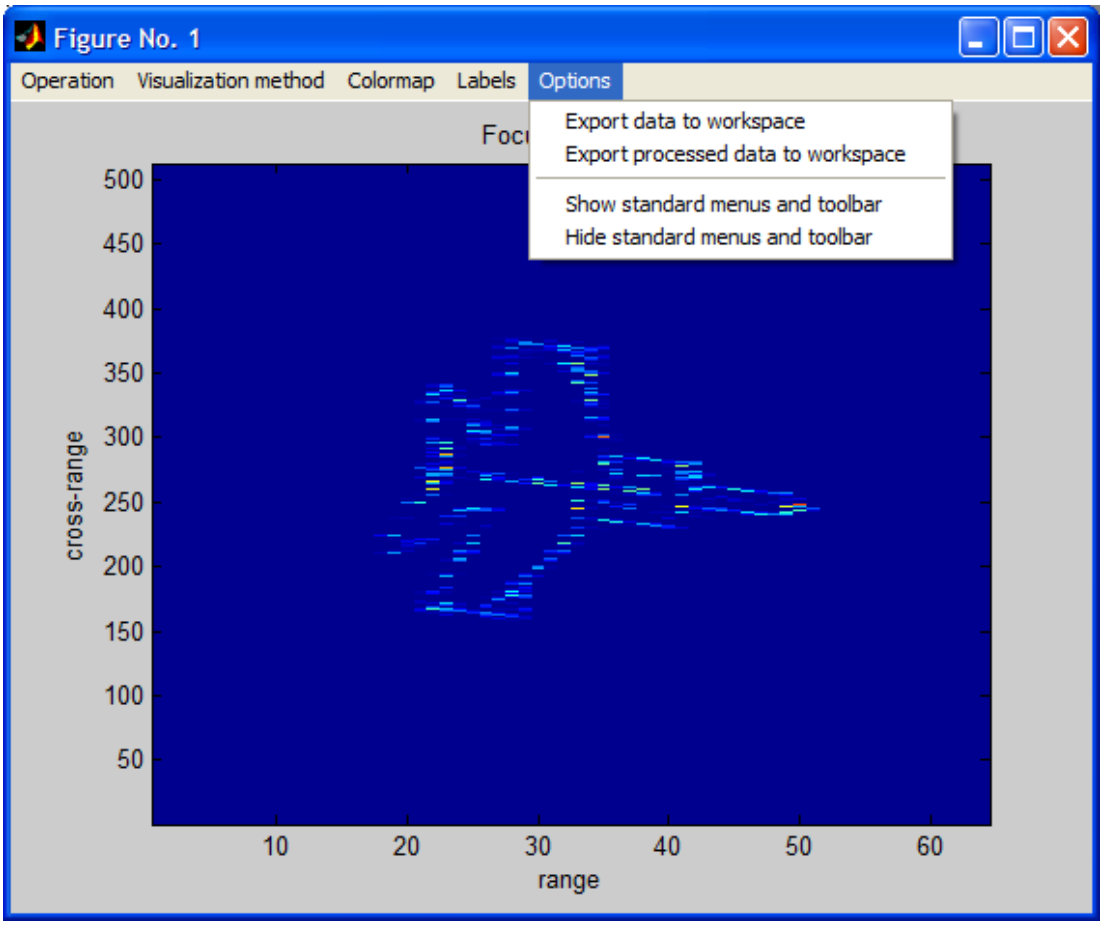

Figure 16: *Data visualization – operations menu.*

The "Options" menu (see Figure 16) is used to export data to MATLAB workspace or to show MATLAB standard figure toolbar.

9 Conclusion

For target recognition applications, mainly those in military surveillance and reconnaissance operations, a blurred SAR/ISAR image of the moving target has to be refocused quickly so that it can be used for real-time target identification. Advanced image focusing methods such as S-method, adaptive S-method and local polynomial Fourier transform method were developed. Based on these three methods, the SAR/ISAR data exploitation toolbox was developed for Geospatial Intelligence (GEOINT) support to Canadian Armed Forces (CAF). The toolbox provides improved target detection and imaging in SAR/ISAR.

In this report, a brief description of these three methods is given. The S-method performs better than the Fourier transform by drastically improving images of fast, maneuvering targets by increasing the SNR in both low and high noise environments. These advantages are the result of the S-method's ability to automatically compensate for quadratic and all even higher-order terms in phase. Thus, targets with constant acceleration will undergo full motion compensation and their point-scatterers will each be localized. The method is also computationally simple, requiring only slight modifications to the existing Fourier transform based algorithm.

However, the S-method is not without significant weaknesses. When the prominent scatterers within the target are very close to each other or when the targets are moving with complicated maneuvers, the undesired cross-terms between scatterers or targets appear as a result of its mutual influence. In order to completely remove the undesired cross-terms, the adaptive S-method is developed. It has been shown that simple strategy for adaptive selection of the frequency window width in the S-method produces excellent results with highly focused radar images and with avoiding undesired interference terms.

The local polynomial Fourier transform-based method produces well-focused radar images of moving targets, without defocusing stationary targets or inducing undesired cross-terms. This method performs accurately even in relatively high noise environments. It is based on the linear signal representation, and it can produce very high-resolution of the radar image with moving target that is close to the resolution of the Fourier transform for radar images with non-moving targets.

In previous studies, the effectiveness of these methods was demonstrated through the application to simulated and experimental data sets. Each method has its own strength and limitation, and the user can explore and compare different data sets using this toolbox. The fastest method is found to be the S-method, followed by the adaptive S-method and then the local polynomial Fourier transform. The S-method generally provides focused image in different SAR/ISAR scenarios, followed by the adaptive S-method and then the local polynomial Fourier transform.

References

[1] Cranos, R. (1997). Combat Identification in the Future: Maintaining the Balance, SPIE Vol.3068, pp. 484.

[2] Schiller, J. (1998). Non-Cooperative Air Target Identification by Radar, RTO Meeting Proceedings 6, NATO Symposium of the RTO Systems Concepts and Integration Panel, Mannheim, Germany.

[3] Van der Heiden, R. (2000). Industry Guidance for Participation in the SET040 TG22 on Non-Cooperative Air Target Identification by Radar, NATO SET040 TG22 working paper NC3A-XLVII-3.

[4] Sparr, T., Hamran, S-E. and Korsbakken, E. (2000). Estimation and correction of complex target motion effects in Inverse Synthetic Aperture imaging of aircraft, IEEE, International Radar Conference, pp. 457, Alexandria USA.

[5] Chen, V. C. and Miceli, W. J. (1998). Time-varying spectral analysis for radar imaging of manoeuvering targets, IEE Proceedings - Radar, Sonar and Navigation, Vol. 145, No. 5, pp. 262-268.

[6] Chen, C. C. and Andrews, H. C. (1980). Target motion induced radar imaging, IEEE Trans. Aerosp. Electron. Syst. No. 16, pp. 2-14.

[7] Wang, Y. X., Hao L. and Chen, V. C. (1998), ISAR motion compensation via adaptive joint time-frequency technique, IEEE Trans. Aerosp. Electron. Syst., Vol. 34, No. 2, pp. 670–677.

[8] Chen, V. C. and Ling, H. (2002). Time–frequency transforms for radar imaging and signal analysis, Artech House, Boston, USA.

[9] Cohen, L. 1995). Time–frequency analysis, Prentice-Hall Inc., New York, USA.

[10] Wehner, D. (1987). High resolution radar, Artech House, Boston, USA.

[11] Walker, J. L. (1980). Range-Doppler imaging of rotating objects, IEEE Trans. Aerosp. Eletron. Syst., AES-16, (l), pp. 23-52.

[12] Thayaparan, T., Lampropoulos, G., Wong, S. K. and Riseborough, E. (2003). Application of adaptive joint time-frequency algorithm for focusing distorted ISAR images from simulated and measured radar data, IEE Proc.-Radar Sonar Navig., Vol 150, No. 2, pp. 213-220.

[13] Thayaparan T. and Kennady S. (2004). Detection of a manoeuvring air target in sea-clutter using joint time–frequency analysis techniques, IEE Proc., Radar Sonar Navig., 2004, 151, (1), pp. 19-30.

[14] Thayaparan, T., Stankovic, L. J., Wernik, C. and Dakovic, M. (2008). Real-Time Motion Compensation, Image Formation and Image Enhancement of Moving Targets in ISAR and SAR Using S-method Based Approach, IET Signal Processing, Vol. 2, No. 3, pp. 247-264.

[15] L. J. Stanković, M. Daković and T. Thayaparan, *Time-Frequency Signal Analysis With Applications*, Artech House, Boston, 2013.

[16] R. Sabry, P. W. Vachon, N. Sandirasegaram, J. Secker, C. Liu, K. E. Mattar, S. Wong and T. Thayaparan, Space-based Radar Products for Military Operations (U): Project 15EL Final Report (U), DRDC-OTTAWA-TR-2013-125, October 2013.

[17] Mattar, K. E., Guertin, R., Schlingmeier, D., Thayaparan, T., Lukowski, T. I, Sabry, R., Secker, J. and Barrie, G. (2013). Makeshift radar reflector trial for search and rescue scenarios. DRDC Ottawa Research Centre, TM-2013-084.

[18] Mattar, K.E., Barrie, G., English, R.A., Liu, C., Sabry, R., Sandirasegaram, N., Secker, J., Thayaparan, T. and Wolfe, J. (2011). An assessment of Synthetic Aperture Radar feature extraction applications, DRDC Ottawa TM 2011-227,DRDC Ottawa.

[19] Vachon, P. W., Barrie, G., Baziuk, W., English, R., Liu, C., Mattar, K., Sabry, R., Sandirasegaram, N., Schlingmeier, D., Secker, J., Thayaparan, T. and Wilcox., C., (2009). Synthetic Aperture Radar exploitation: RDE Groups' perspective, DRDC Ottawa TR 2009-194.

[20] Thayaparan, T. and Brinkman, W. (2009). Focusing distorted ISAR images using fast adaptive joint time-frequency and 3-dimensional motion detection on experimental radar data, DRDC Ottawa TM 2009-281, 46.

[21] Thayaparan, T., Stankovic, L. J., Dakovic, M. and Popovic, V. (2009). Micro-Doppler signal estimation for rotating targets from a fraction of the period, DRDC Ottawa TM 2009-290.

[22] Thayaparan, T. and Wernik, C. (2006). A Novel S-Method Based Approach for Real-Time Motion Compensation, Image Formation and Image Enhancement of Moving Targets in ISAR and SAR, DRDC Ottawa TR 2006-246.

[23] Thayaparan, T. (2006). ISAR motion compensation using the registration-restoration-fusion method, DRDC Ottawa, TM 2006-131.

[24] Thayaparan, T. (2006). Focusing ISAR Images using the Adaptive Local Polynomial Fourier, TM 2006-185.

[25] Thayaparan, T. (2006). Separation of target rigid body and micro-Doppler effects in ISAR/SAR, DRDC Ottawa, TM 2006-187.

[26] Thayaparan, T. and Abrol, S. (2005). Micro-Doppler Analysis of Rotating Target in SAR, DRDC Ottawa TM 2005-204, December 2005.

[27] Thayaparan, T., Abrol, S. and Riseborough, E. (2004). Micro-Doppler radar signatures for intelligent target recognition, DRDC Ottawa TM 2004-170, 57 pages.

[28] Wong, S. Riseborough, E., Duff, G. and Thayaparan, T. (2004). Experimental and numerical investigations in the distortion of ISAR images and time-frequency algorithms development for ISAR imaging process, DRDC Ottawa ECR 2004-169.

[29] Thayaparan, T. and Lampropoulos, G. (2003). A new approach in time-frequency analysis with applications to experimental high resolution radar, DRDC Ottawa TR 2003-187, December 2003.

[30] Thayaparan, T., Wong, S. K., Riseborough, E. and Lampropoulos, G. (2003). Focusing ISAR images using adaptive joint time-frequency algorithm on simulated and experimental radar data, DRDC Ottawa TM 2003-089.

[31] Thayaparan, T., Stankovic, L. J., Amin. M., Chen. V., Cohen, L. and Boashash, B. (2010). Editorial: Time-frequency approach to radar detection, imaging, and classofication, IET Signal Processing, Vol. 4, No. 3, pp. 197-200.

[32] Thayaparan, T., Stankovic, L. J., Amin. M., Chen. V., Cohen, L. and Boashash, B. (2010). Editorial: Time-frequency approach to radar detection, imaging, and classofication, IET Signal Processing, Vol. 4, No. 4, pp. 325-328.

[33] Popovic, V., Djurovic, I., Stankovic, L. J., Thayaparan, T. and Dakovic, M. (2010), Autofocusing of SAR images based on parameters estimated from the PHAF, Signal Processing, Vol. 90, No. 5, pp. 1,382-1,391.

[34] Thayaparan, T., Brinkman, W. and Lampropoulos, G. (2010). Inverse synthetic aperture radar image focusing using fast AJTF and 3-dimensional motion detection on experimental radar data, IET Signal Processing, Vol. 4, No. 4, pp. 382-394.

[35] Brinkman, W. and Thayaparan, T. (2010). Focusing ISAR images using the adaptive joint time-frequency algorithm optimized with the genetic algorithm and particle swarm optimization algorithm - comparison and results, IET Signal Processing, Vol. 4, No. 4, pp. 329-342.

[36] Orovic, I., Stankovic, S., Thayaparan, T. and Stankovic, L. J. (2010). Multiwindow S-method for Instantaneous Frequency Estimation and its Application in Radar Signal Analysis, IET Signal Processing, Vol. 4, No. 4, pp. 363-370.

[37] Djurovic, I., Ioana, C., Thayaparan, T., Stankovic, L. J., Wang, P., Popovic, V. and Simeunovic, M. (2010). Cubic-phase function evaluation for multicomponent signals, IET Signal Processing, Vol. 4, No. 4, pp. 371-381.

[38] Thayaparan, T., Lampropoulos, G. and Stankovic, L. J. (2008), Motion compensation in ISAR imaging using the registration-restoration-fusion approach, IET Signal Processing, Vol. 2, No. 3, pp. 223-236.

[39] Thayaparan, T., Stankovic, L. J., Wernik, C. and Dakovic, M. (2008). Real-Time Motion Compensation, Image Formation and Image Enhancement of Moving Targets in ISAR and SAR Using S-method Based Approach, IET Signal Processing, Vol. 2, No. 3, pp. 247-264.

[40] Thayaparan, T., Frangos, P., Stankovic, L. J., Stergioulas, L. and Lazarov, A. D., (2008) Editorial: Signal Processing Techniques for Inverse Synthetic Aperture Radar (ISAR) and Feature Extraction, IET Signal Processing, Vol. 2, No. 3, pp. 189-191.

[41] Djurovic, I., Thayaparan, T. and Stankovic, L. J. (2008). SAR Imaging of Moving Targets using Polynomial FT, IET Signal Processing, Vol. 2, No. 3, pp. 237-246.

[42] Stankovic, L. J., Thayaparan, T., Popovic, V., Djurovic, I. and Dakovic, M. (2008). Adaptive S-Method for SAR/ISAR Imaging, , EURASIP Journal on Applied Signal Processing, Volume 2008, Article ID 593216, pp. 1-10.

[43] Djurovic, I., Thayaparan, T. and Stankovic, L. J. (2006). Adaptive local polynomial Fourier transform in ISAR, EURASIP Journal on Applied Signal Processing, Vol. 2006, Article ID 36093, pp. 1-15.

[44] Lampropoulos, G. A., Thayaparan, T. and Xie, N. (2006). Fusion of Time Frequency Distributions and Applications to Radar Signals, Journal of Electronic Imaging, Vol. 15, Issue 2, pp. 1-17.

[45] Thayaparan, T., Lampropoulos, G., Wong, S. K. and Riseborough, E. (2003). Application of adaptive joint time-frequency algorithm for focusing distorted ISAR images from simu-lated and measured radar data, IEE Proc.-Radar Sonar Navig., Vol 150, No. 2, pp. 213-220.

[46] P. Suresh, T. Thayaparan and K. Venkataramaniah, Micro-Doppler Analysis of Rotating Targets using the Adaptive S- method, International Radar Symposium India 2011, 30 Nov-4 Dec 2011, Bangalore, India.

[47] Thayaparan, T., Djurovic, I. and Stankovic, L. J, (2006), Focusing distorted ISAR images using Adaptive Local Polynomial Fourier Transform, International Radar Symposium - IRS 2006, 24-26 May, Krakow, Poland, pp. 533-536.

[48] Thayaparan, T., Range-Doppler Radar Imaging and Motion Compensation, International Radar Symposium India 2011, 30 Nov-4 Dec 2011, Bangalore, India.

[49] Thayaparan, T., Non-stationary Radar Signal Analysis – Time-Frequency Approach, International Radar Symposium India 2011, 30 Nov-4 Dec 2011, Bangalore, India.

[50] Piorkowska, J. and Thayaparan, T. (2011). Processing and analysis of polarimetric ship signatures using high-resolution using S-method and local polynomial Fourier transform, Coop Student Work-Term Report, DRDC Ottawa.

[51] Stankovic, L. J., 'A method for time–frequency analysis', IEEE Trans. Signal Process., 1994, 42, pp. 225–229.

[52] Stankovic, S. and Stankovic, L. J., "An architecture for the realization of a system for time-frequency signal analysis", IEEE Trans. on Circuits and Systems, Part II, no.7, pp. 1211-1217, July 1997.

[53] Stankovic, L. J., Ivanovic, V. and Petrovic, Z., "Unified approach to the noise analysis in the Wigner distribution and Spectrogram", Annales Telecomm., pp. 585-594, Nov./Dec. 1996.

[54] Gonzalez, R. C. and Woods, R. E., Digital image processing, Prentice Hall, 2002.

[55] Katkovnik, V. (1995). A new form of the Fourier transform for time-frequency estimation, Signal Processing, Vol. 47, No. 2, pp. 187-200.

[56] Katkovnik, V. (1996). Local polynomial approximation of the instantaneous frequency: Asymptotic accuracy, Signal Processing, Vol. 52, No. 3, pp. 343-356.

[57] Thayaparan, T. L., Stankovic, J., Suresh, P., Venkataramaniah, K., and S. SivaSankaraSai. (2010). Focusing ISAR images of moving targets in real-time using time-frequency-based method, International Radar Symposium 2010, June 16-18, Lithuania.

[58] Suresh, P., Thayaparan, T., Venkataramaniah, K., SivaSankaraSai, S. and Sridharan, K. S. (2009). Analysis of micro-Doppler radar signatures in SAR using S-method-based, International Radar Symposium India- 2009, December 8-11, Bangalore, India.

[59] Thayaparan, T., Stankovic, L. J, Dakovic, M., Djurovic, I. and Popovic, V. (2009). Image Enhancement and Motion Compensation of Moving Targets in ISAR using S-Method, ISBN: 2-912328-55-1 October 12-16, Bordeaux, France.

[60] Thayaparan, T., Darkovic, M., and Stankovic, L. J. (2006), Focusing distorted ISAR images using the s-method, pp. 121-125, May 7, IEEE CCECE 2006 Conference, Ottawa, Canada.

[61 Stankovic, L. J., Thayaparan T., and Dakovic, M. (2006), Improvement of the Fast Moving Targets Presentation in ISAR by Using the S-Method, September 4-8, 2006, Florence, Italy, papers in CD, EURASIC symposium 2006.

[62] Ivanovic, V. N., Stojanovic, R. and Stankovic, L. J. (2006), Multiple clock cycle architecture for the VLSI design of a system for time-frequency analysis, EURASIP Journal on Applied SP, Special Issue on Design Methods for DSP Systems, Article ID 60613, pp. 1-18.

This page intentionally left blank.

DOCUMENT CONTROL DATA

(Security markings for the title, abstract and indexing annotation must be entered when the document is Classified or Designated.)

1. ORIGINATOR (The name and address of the organization preparing the document. Organizations for whom the document was prepared, e.g. Centre sponsoring a contractor's report, or tasking agency, are entered in section 8.)

DRDC – Ottawa Research Centre
3701 Carling Avenue, Ottawa ON K1A 0Z4, Canada

2a. SECURITY MARKING (Overall security marking of the document, including supplemental markings if applicable.)

UNCLASSIFIED

2b. CONTROLLED GOODS

(NON-CONTROLLED GOODS)
DMC A
REVIEW: GCEC APRIL 2011

3. TITLE (The complete document title as indicated on the title page. Its classification should be indicated by the appropriate abbreviation (S, C or U) in parentheses after the title.)

SAR/ISAR data exploitation toolbox for focusing moving targets

4. AUTHORS (Last name, followed by initials – ranks, titles, etc. not to be used.)

Thayaparan, T.

5. DATE OF PUBLICATION (Month and year of publication of document.)	6a. NO. OF PAGES (Total containing information. Include Annexes, Appendices, etc.)	6b. NO. OF REFS (Total cited in document.)
April 2015	52	62

7. DESCRIPTIVE NOTES (The category of the document, e.g. technical report, technical note or memorandum. If appropriate, enter the type of report, e.g. interim, progress, summary, annual or final. Give the inclusive dates when a specific reporting period is covered.)

Scientific Report

8. SPONSORING ACTIVITY (The name of the department project office or laboratory sponsoring the research and development – include address.)

DRDC – Ottawa Research Centre
3701 Carling Avenue, Ottawa ON K1A 0Z4, Canada

9a. PROJECT OR GRANT NO. (If appropriate, the applicable research and development project or grant number under which the document was written. Please specify whether project or grant.)	9b. CONTRACT NO. (If appropriate, the applicable number under which the document was written.)
15dp	

10a. ORIGINATOR'S DOCUMENT NUMBER (The official document number by which the document is identified by the originating activity. This number must be unique to this document.)	10b. OTHER DOCUMENT NO(s). (Any other numbers which may be assigned this document either by the originator or by the sponsor.)
DRDC-RDDC-2015-R018	

11. DOCUMENT AVAILABILITY (Any limitations on further dissemination of the document, other than those imposed by security classification.)

(X) Unlimited distribution
( ) Defence departments and defence contractors; further distribution only as approved
( ) Defence departments and Canadian defence contractors; further distribution only as approved
( ) Government departments and agencies; further distribution only as approved
( ) Defence departments; further distribution only as approved
( ) Other (please specify):

12. DOCUMENT ANNOUNCEMENT (Any limitation to the bibliographic announcement of this document. This will normally correspond to the Document Availability (11). However, where further distribution (beyond the audience specified in (11)) is possible, a wider announcement audience may be selected.)

Unlimited

13. ABSTRACT (A brief and factual summary of the document. It may also appear elsewhere in the body of the document itself. It is highly desirable that the abstract of classified documents be unclassified. Each paragraph of the abstract shall begin with an indication of the security classification of the information in the paragraph (unless the document itself is unclassified) represented as (S), (C), or (U). It is not necessary to include here abstracts in both official languages unless the text is bilingual.)

The commonly used technique for SAR/ISAR imaging of a moving target is a Fourier-based image formation, which assumes time invariance of the Doppler frequency to resolve the image in the cross-range. However, in real-world ISAR/SAR imaging scenarios, when a target exhibits complex motion such as rotation, acceleration, or manoeuvring, standard Fourier-based methods can cause range-Doppler image blur-ring and leave the image unrecognizable. For target recognition applications, mainly those in military surveillance and reconnaissance operations, a blurred ISAR image of the moving target has to be refocused quickly so that it can be used for real-time target identification. Subsequently, advanced image focusing (or refocusing distorted images) methods such as, S-method, adaptive S-method and local polynomial Four-ier transform method were developed. These three image focusing and motion com-pensation algorithms were successfully tested and validated with numerous measured ocean and air targets using airborne, space-borne, and ground-based sensors. Based on these three algorithms, the SAR/ISAR data exploitation toolbox was developed for Geospatial Intelligence (GEOINT) support to the Canadian Armed Forces (CAF).

14. KEYWORDS, DESCRIPTORS or IDENTIFIERS (Technically meaningful terms or short phrases that characterize a document and could be helpful in cataloguing the document. They should be selected so that no security classification is required. Identifiers, such as equipment model designation, trade name, military project code name, geographic location may also be included. If possible keywords should be selected from a published thesaurus. e.g. Thesaurus of Engineering and Scientific Terms (TEST) and that thesaurus identified. If it is not possible to select indexing terms which are Unclassified, the classification of each should be indicated as with the title.)

Inverse Synthetic Aperture Radar; Synthetic Aperture Radar; Non-Stationary Signal; Fourier Transform; Time-Frequency Analysis; Short-Time Fourier Transform; Wigner Distribution; S-Method; Adaptive S-Method; Local Polynomial Fourier Transform; Geospatial Intelligence.